CENTRO BRASILEIRO DE PESQUISAS FÍSICAS
http://www.cbpf.br

MICROSCOPIA ELETRÔNICA DE VARREDURA

ANDRÉ LUIZ PINTO

CBPF

Roteiro
Aplicações da Microscopia à Nanotecnologia

- Introdução
  - O que é Nanotecnologia?
  - O arsenal disponível para “ver” a matéria condensada
- Histórico do Mundo da Microscopia
- Microscópio Eletrônico de Transmissão
- Microscópio Eletrônico de Varredura
- Nanolitografia por por Feixe de Elétrons
- A Utilização de Feixe de Íons
- Comentários Finais
  - LabNano

Opções para visualizar a microestrutura

- Aumento x Resolução (lateral)

- Olho humano – 0,1 mm
- Microscopia Ótica – 0,5 μm
- Microscópio Eletrônico de Varredura (MEV) – 1 - 4 ηm
- Microscópio Eletrônico de Transmissão (MET) – 0,8 - 1,4 Å
- Microscópio de Ponta de Prova (SPM) – 0,3 Å

Interação Elétron-Amostra

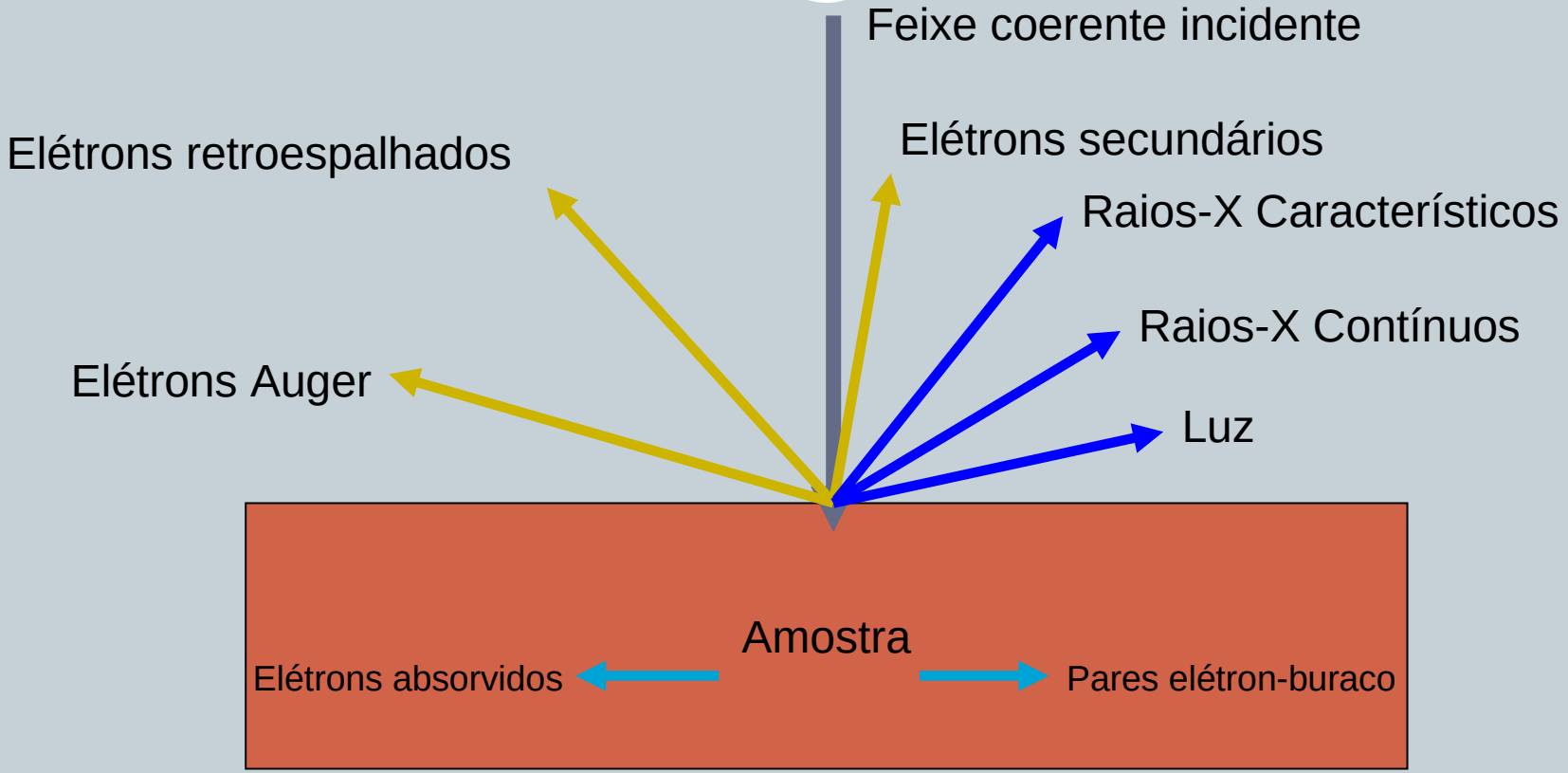

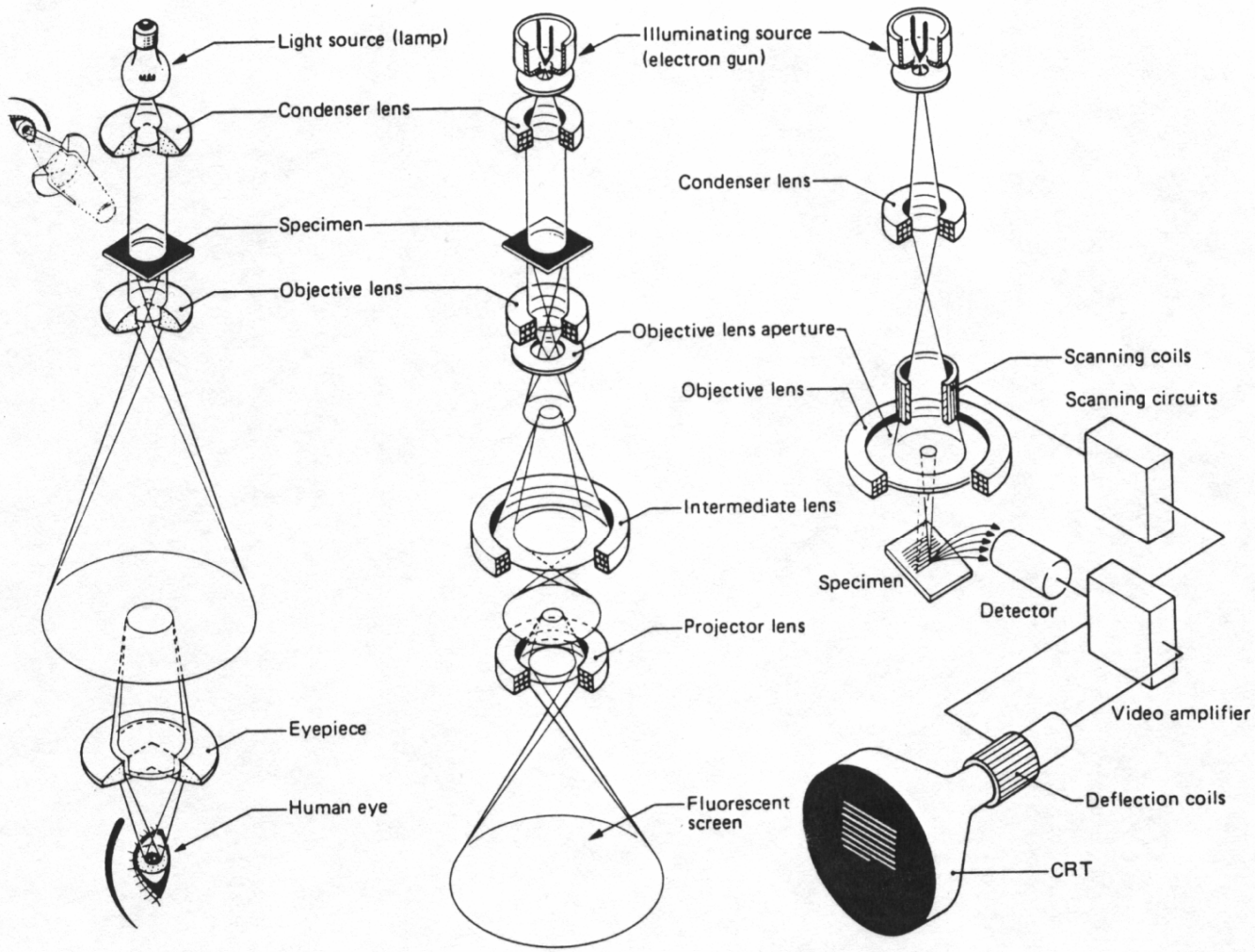

Optical microscope

Transmission electron microscope

Scanning electron microscope

Image formation

Jeol

Microscopia Eletrônica de Varredura

Raith

Microscopia Eletrônica de Varredura

Jeol

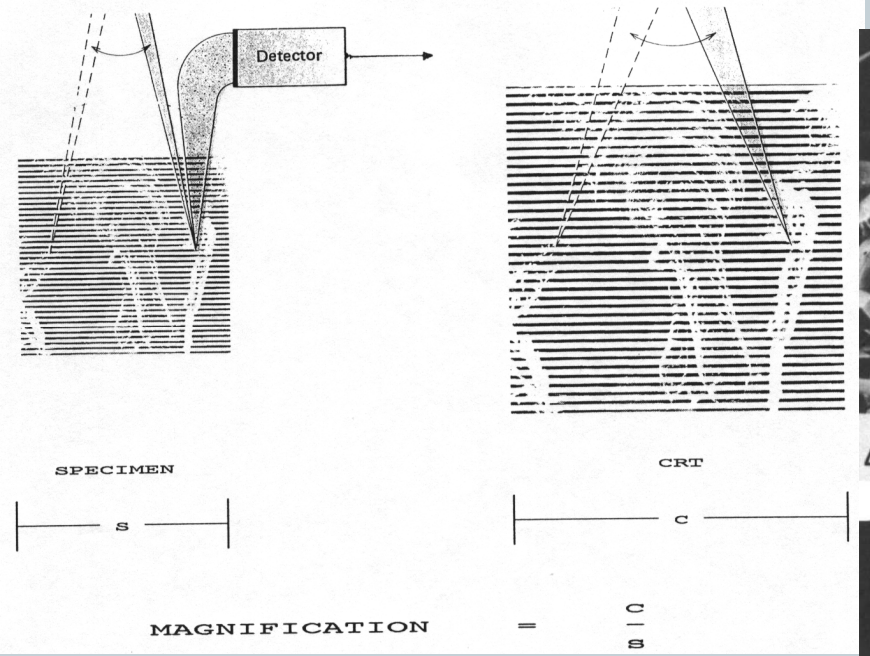

Goldstein et alli, 2003

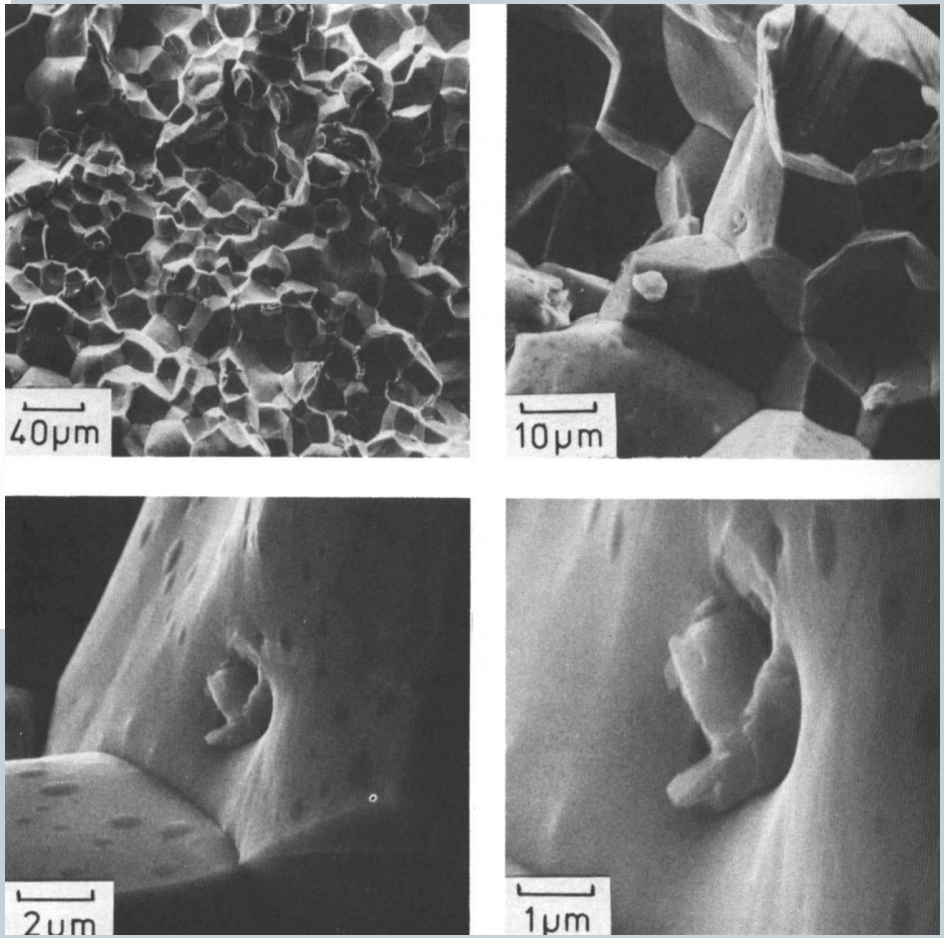

No MEV, o aumento é dado pela relação entre as dimensões varridas na amostra e as dimensões da tela.

“Spot Size” e Resolução

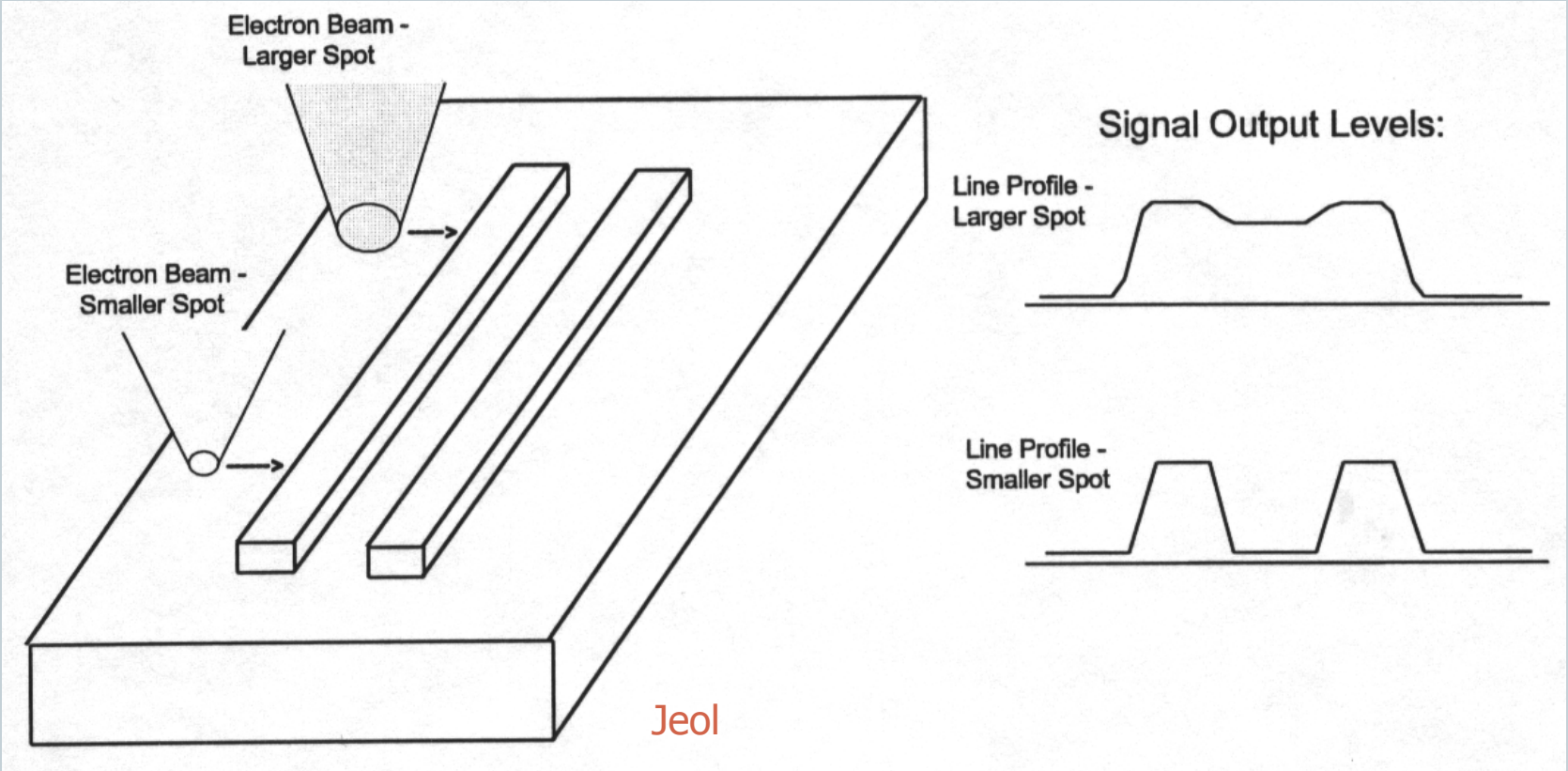

Goldstein et alli, 2003

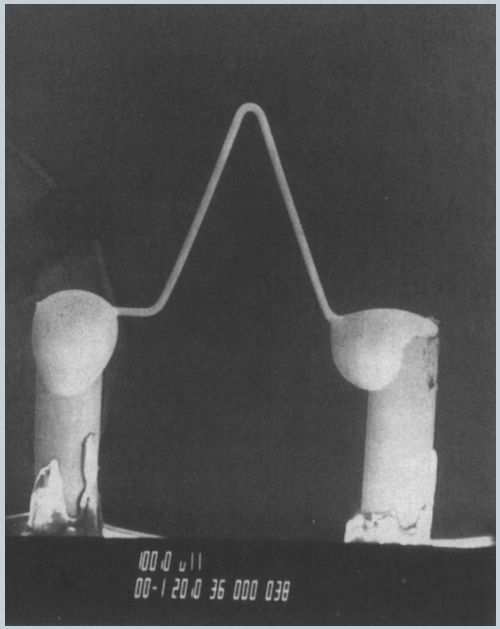

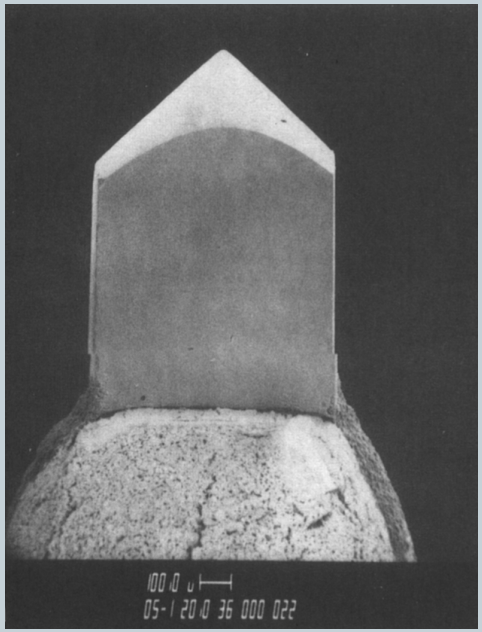

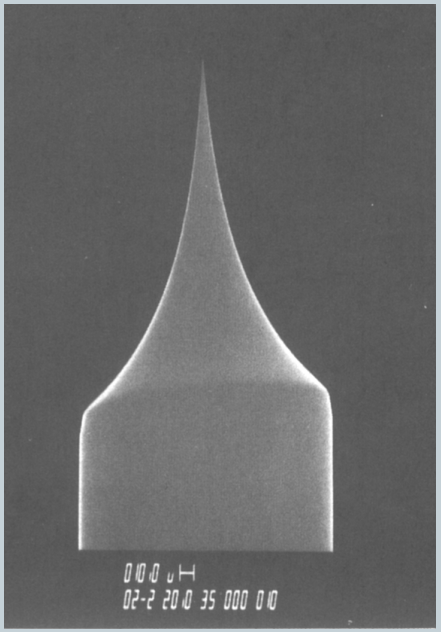

TABLE 5.1. Characteristics of the Three Principal Sources Operating at 100 kV

	Units	Tungsten	LaB_6	Field Emission
Work function, Φ	eV	4.5	2.4	4.5
Richardson's constant	A/m^2K^2	6×10^5	4×10^5	
Operating temperature	K	2700	1700	300
Current density	A/m^2	5×10^4	10^6	10^{10}
Crossover size	µm	50	10	<0.01
Brightness	A/m^2sr	10^9	5×10^{10}	10^{13}
Energy spread	eV	3	1.5	0.3
Emission current stability	%/hr	<1	<1	5
Vacuum	Pa	10^{-2}	10^{-4}	10^{-8}
Lifetime	hr	100	500	>1000

Williams e Carter, 2009

Formas de relaxação de um átomo ionizado pelo feixe

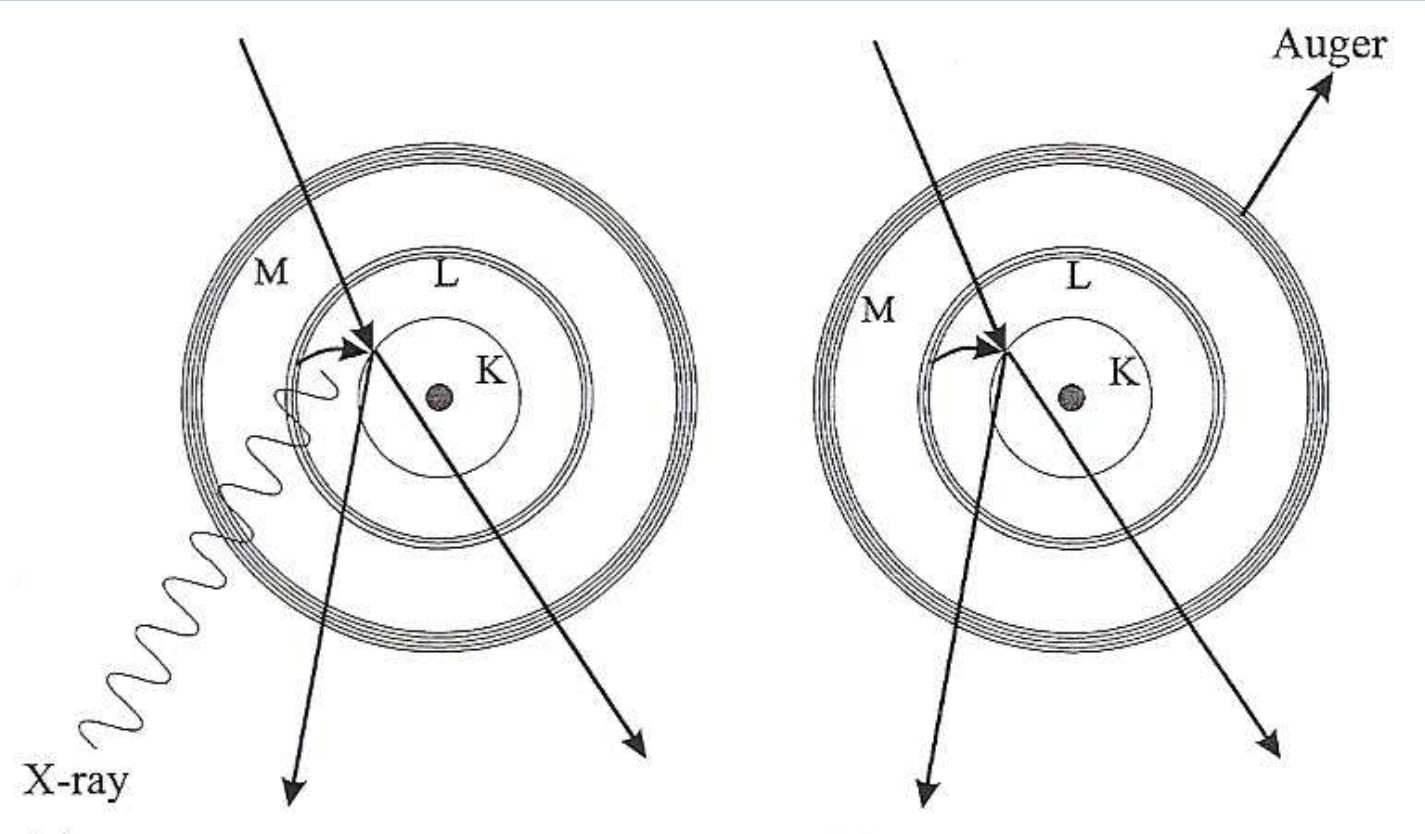

Goodhew et all

Imagem de Elétrons Secundários

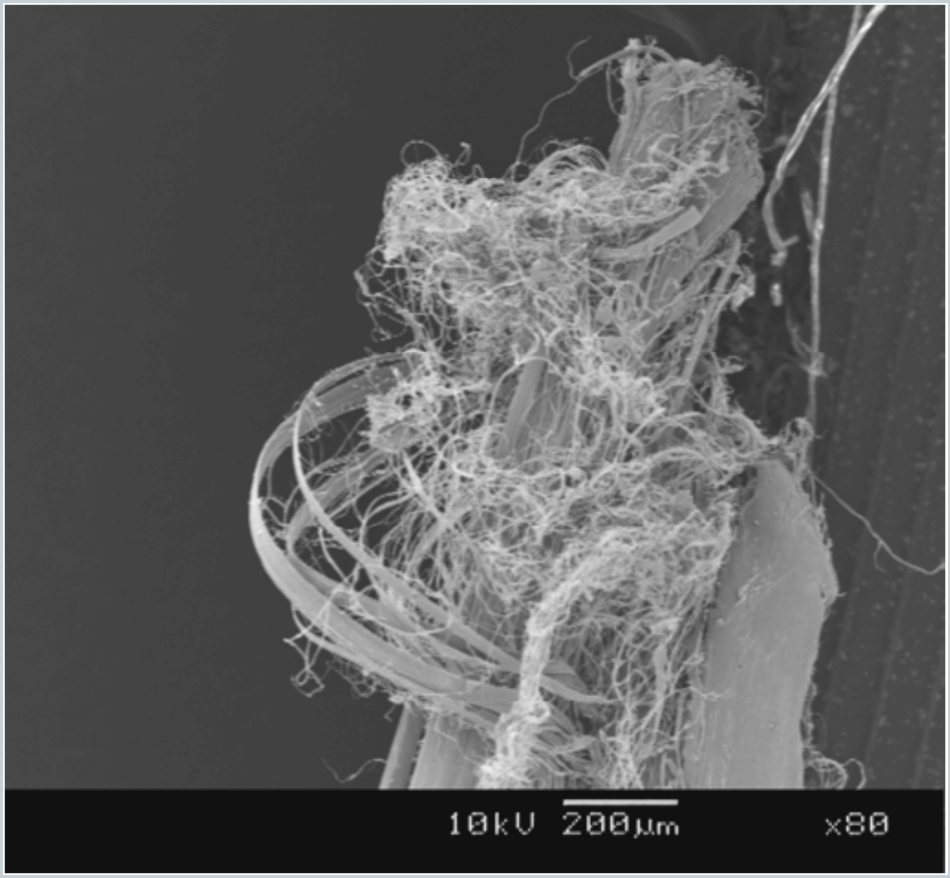

Placa de Armodon (UHMW-PP) submetida a Impacto balístico.

Elétrons Retroespalhados

- Espalhamento elástico de Rutherford para um ângulo maior do que θ:

$$\sigma(\rangle\theta) = 1{,}62x10^{-20}\frac{Z^2}{E}ctg^2\frac{\theta}{2}$$

  - E é a energia do feixe
  - Z é o número atômico

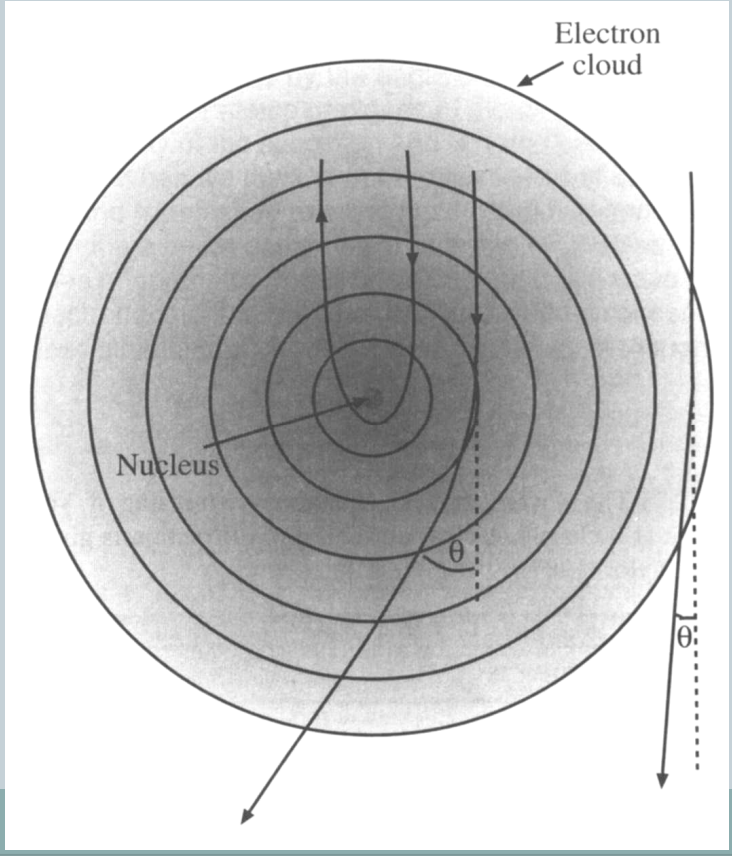

Imagem de Elétrons Retroespalhados

- Contraste de Z

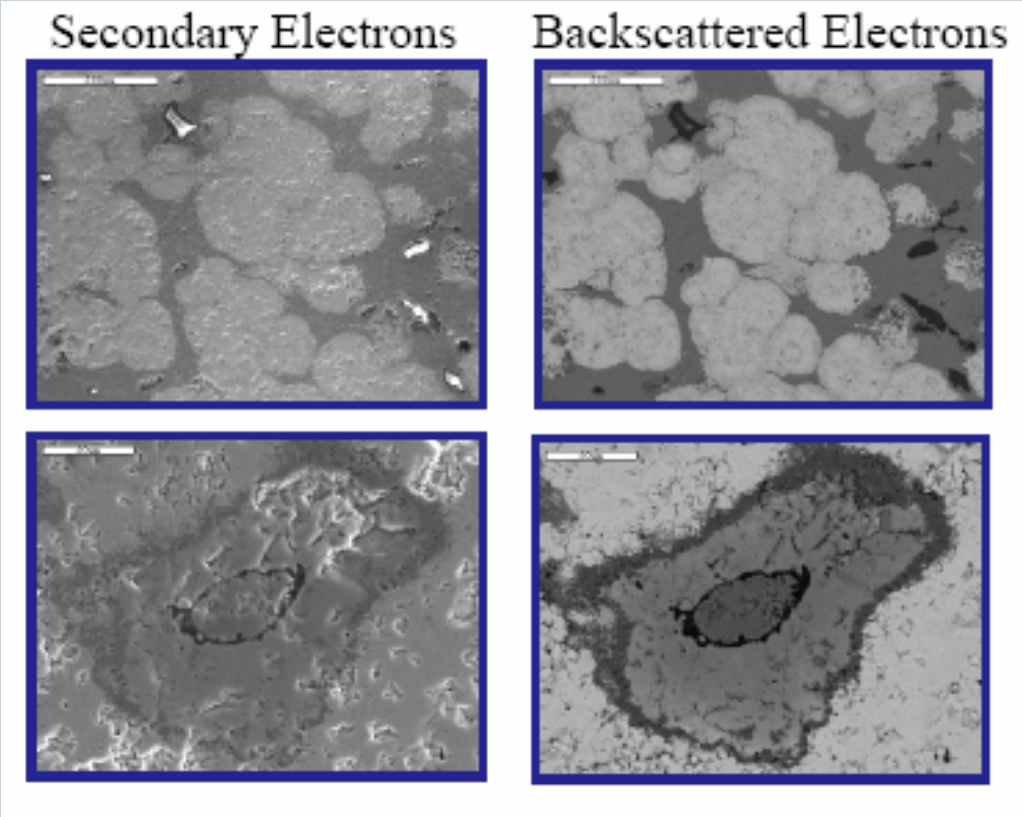

Goldstein et alli, 2003

Raios X Característicos

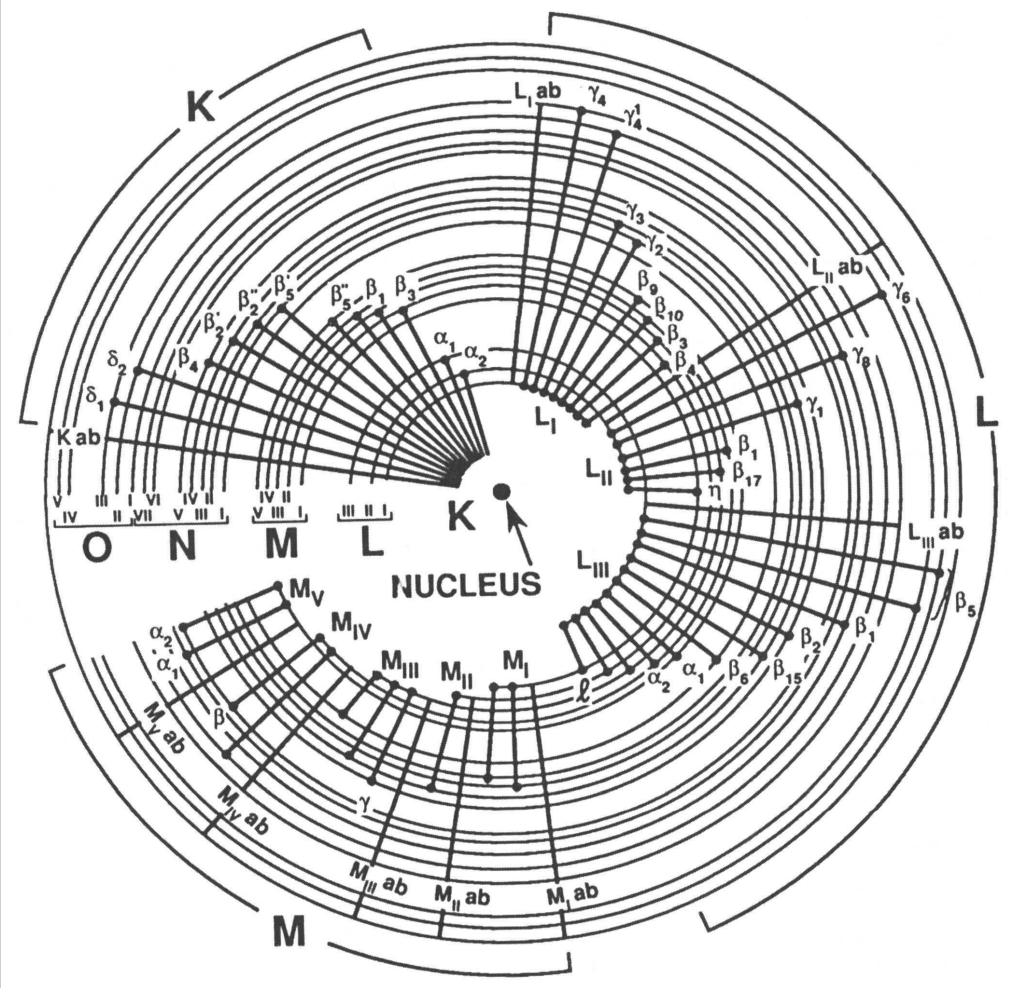

Jeol

Espectro de EDS

- Permite a análise qualitativa da composição química
- Permite a realização de mapeamentos para localização de elementos químicos

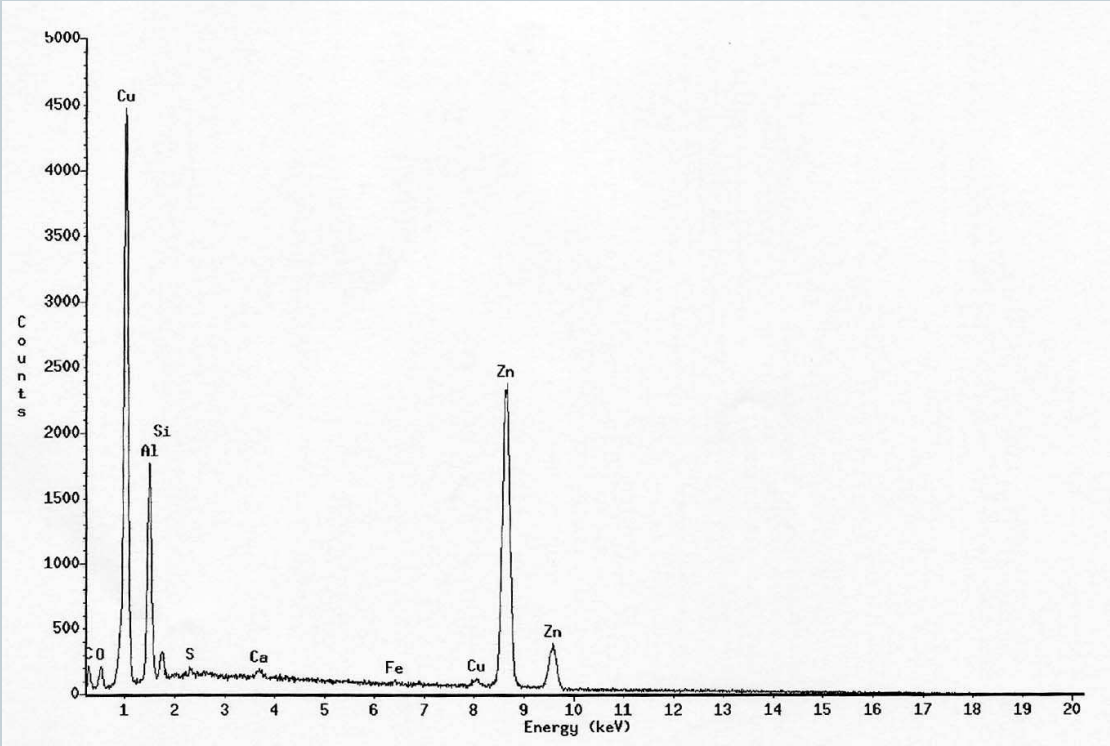

Resolução e origem

- e^- Secundários

  ~ 1 ηm
- e^- Retroespalhados

  ~ 0,1 μm
- EDS

  ~ 1 μm

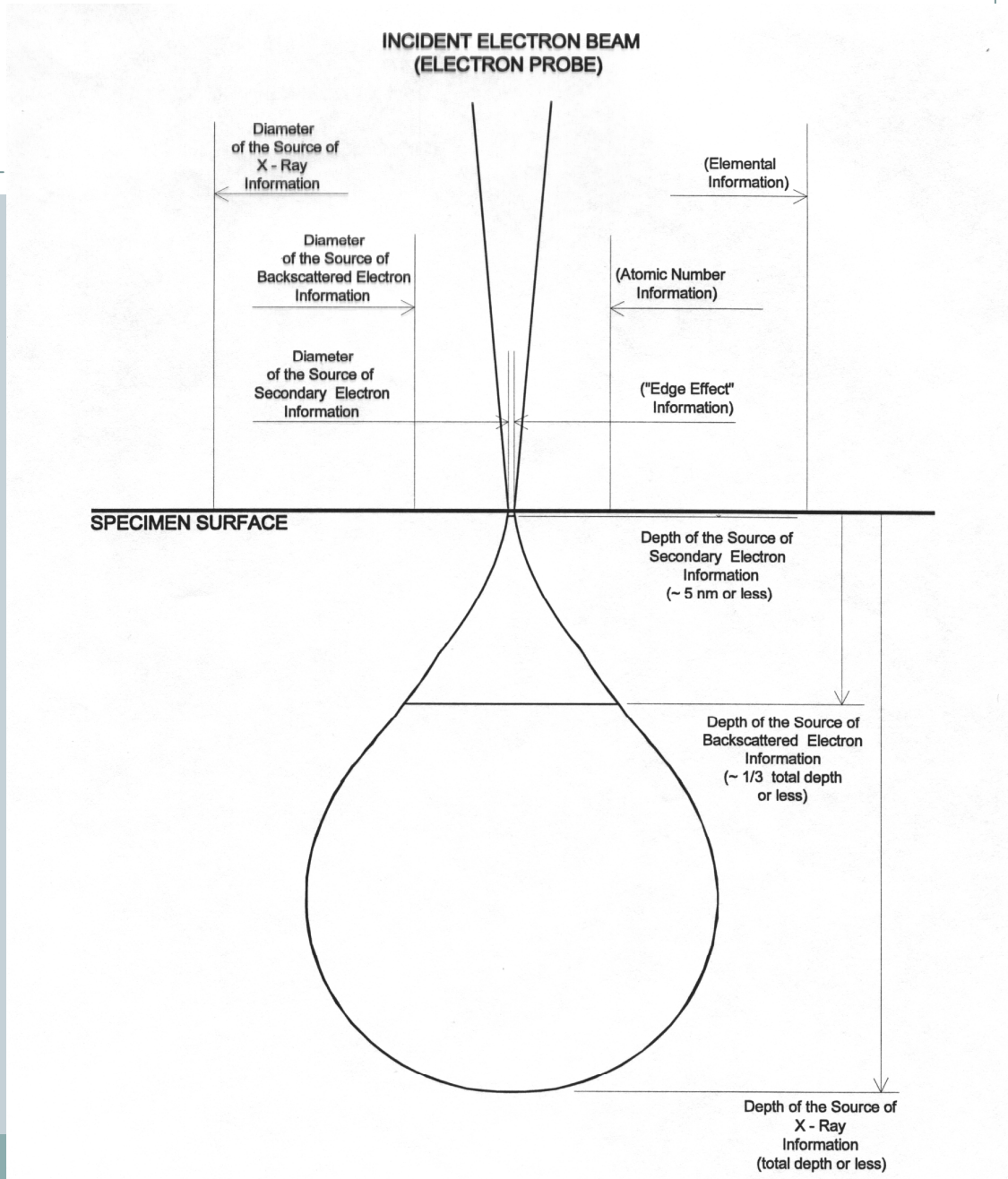

Elétrons Secundários
Os vários sinais

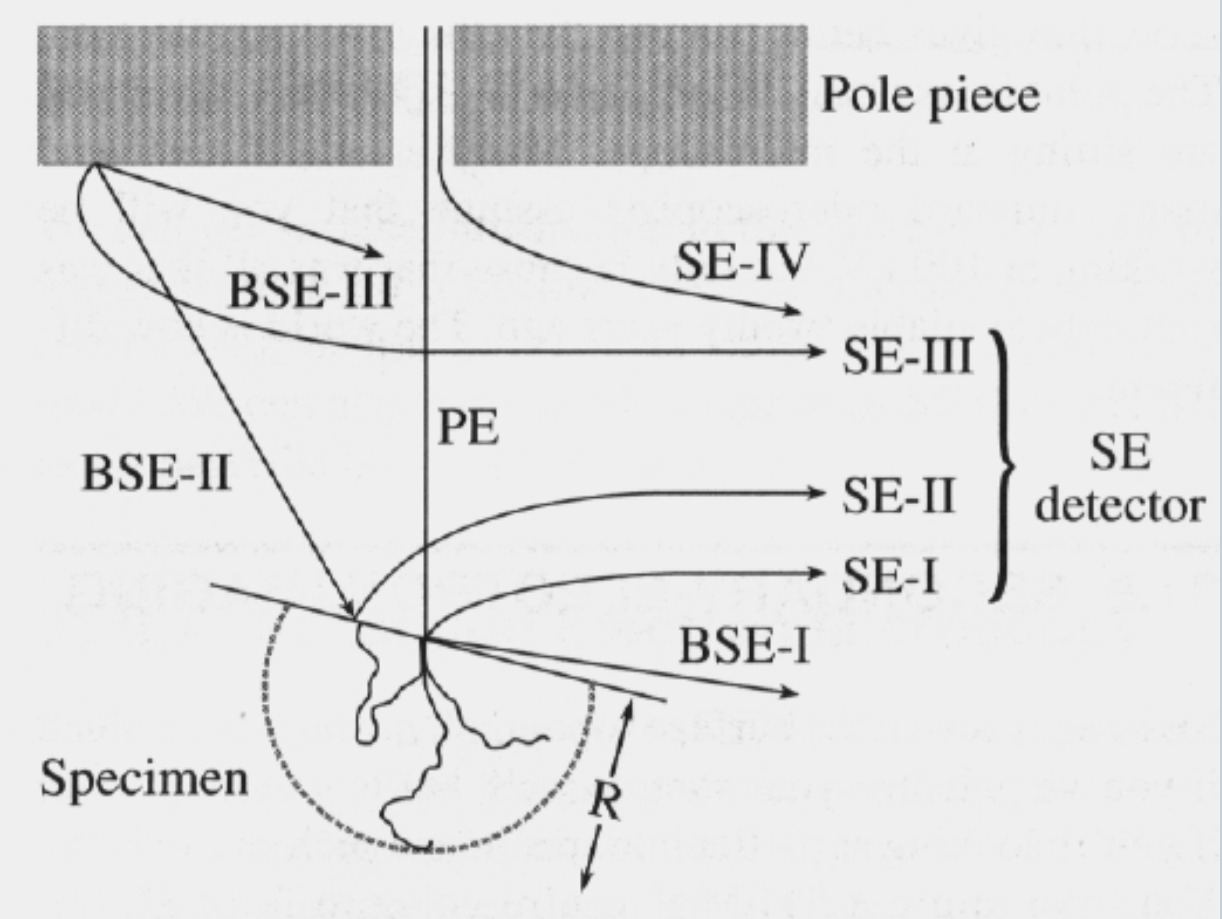

Detectores de Elétrons Secundários

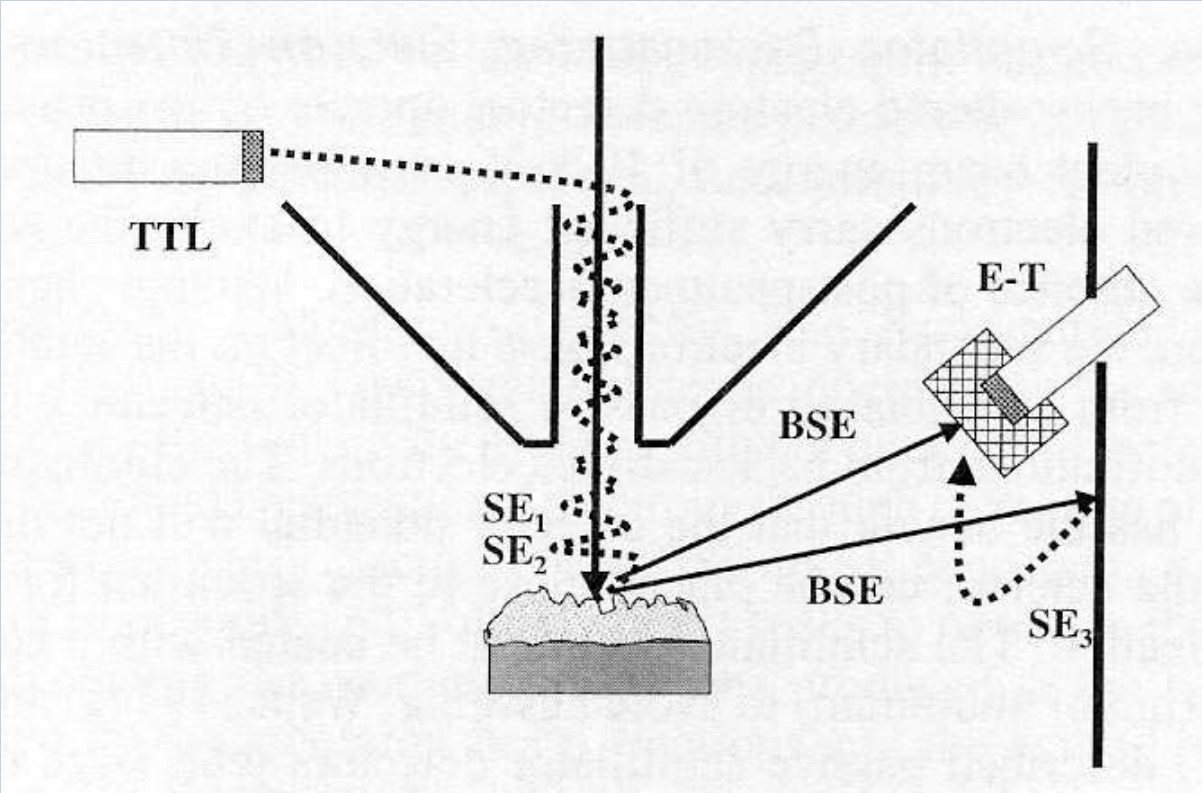

Uma visão comparativa dos vários sinais

SE + BSE

SE + BSE

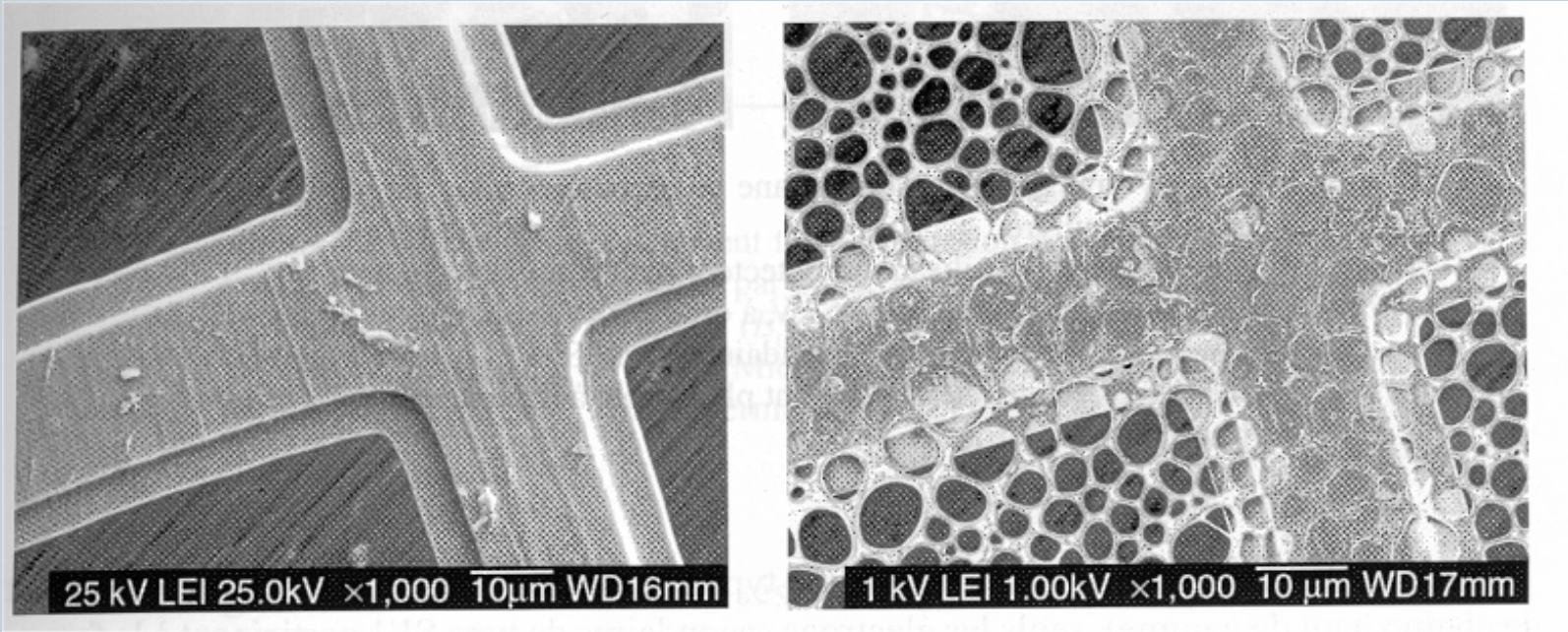

E_0 influence on the SE image

FEI

lateral detector

Uma visão comparativa dos vários sinais

SE

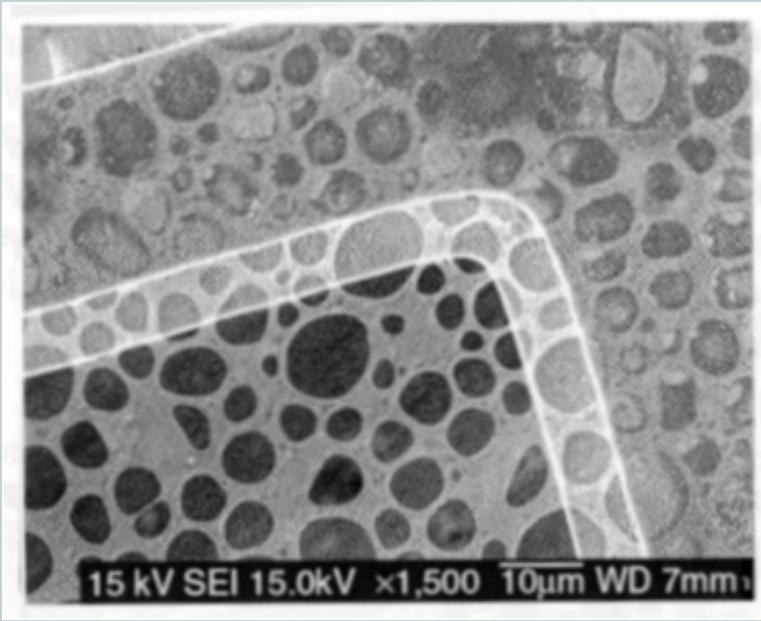

SE

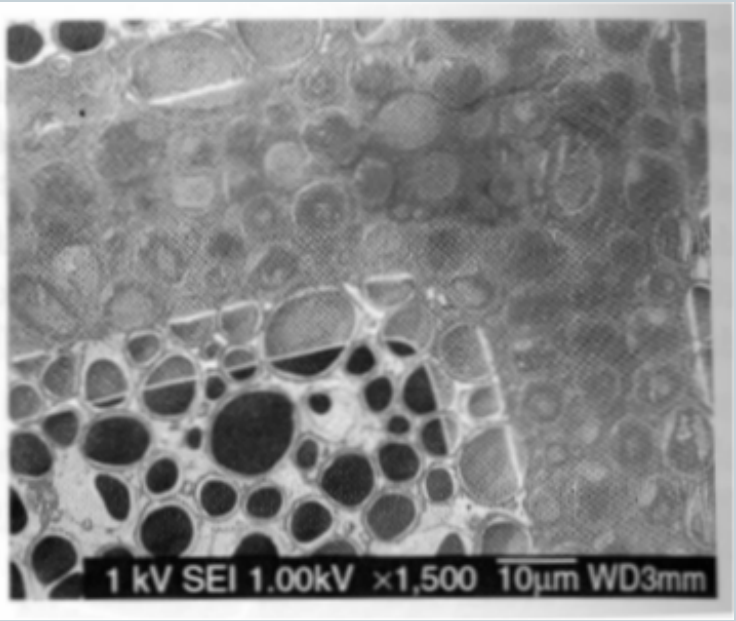

FEI

E_0 influence on the SE image

In-lens detector

Uma visão comparativa dos vários sinais

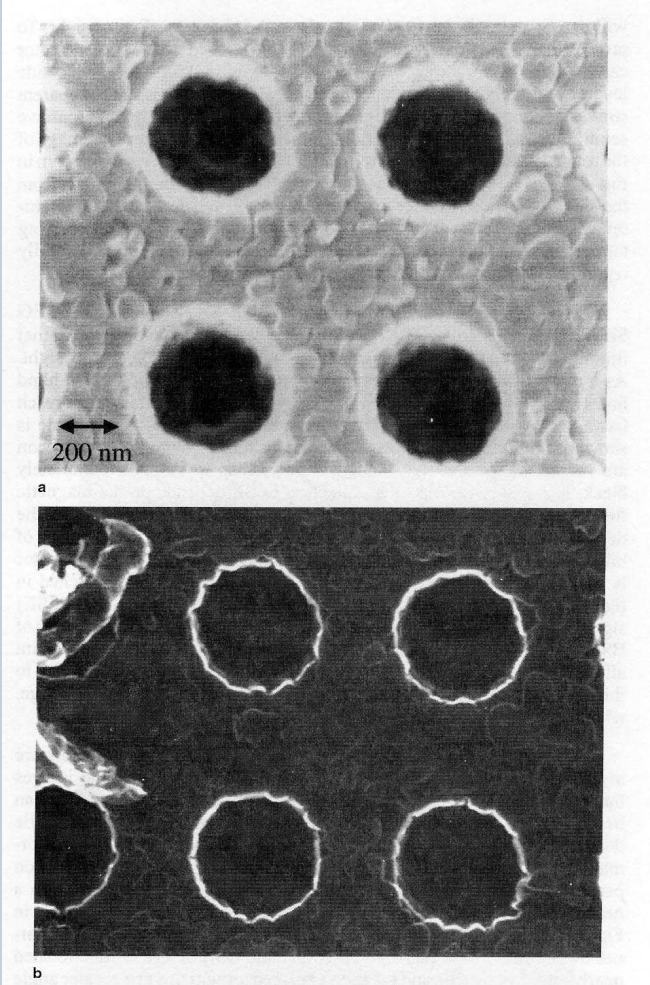

E-T lateral

E-T in lens

FEI

Revestimento nc-TiC/a-C

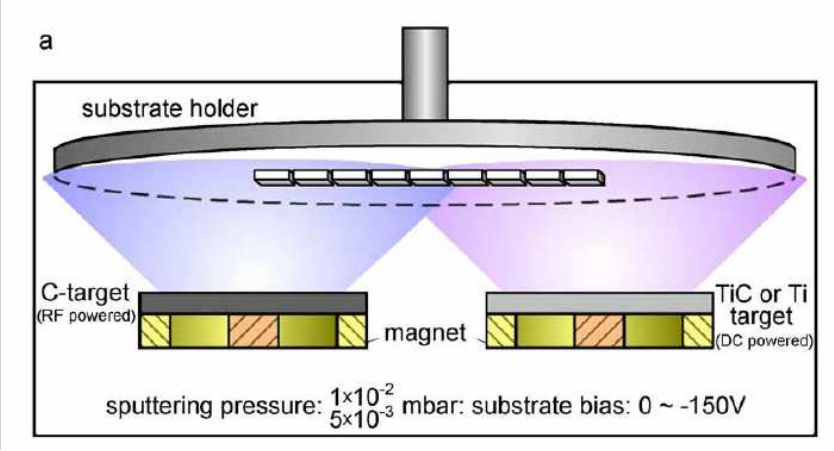

Pei et al. (2005)

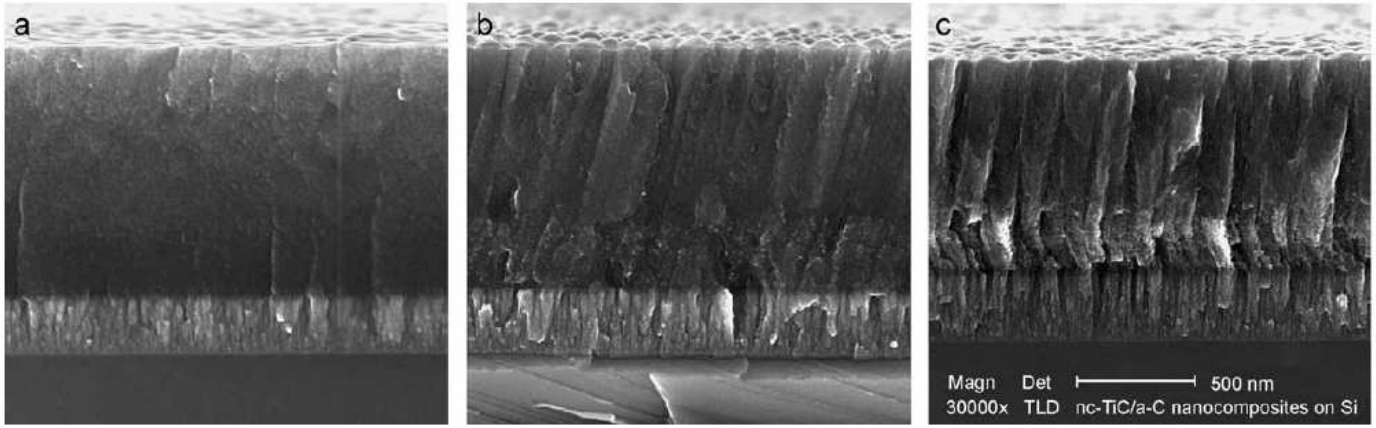

Fig. 2. SEM micrographs of the fractured cross-sections showing the transition from glassy to columnar growth of nc-TiC/a-C coatings with Ti content (at.%) of (a) 10, (b) 17 and (c) 34.

Revestimento nc-TiC/a-C

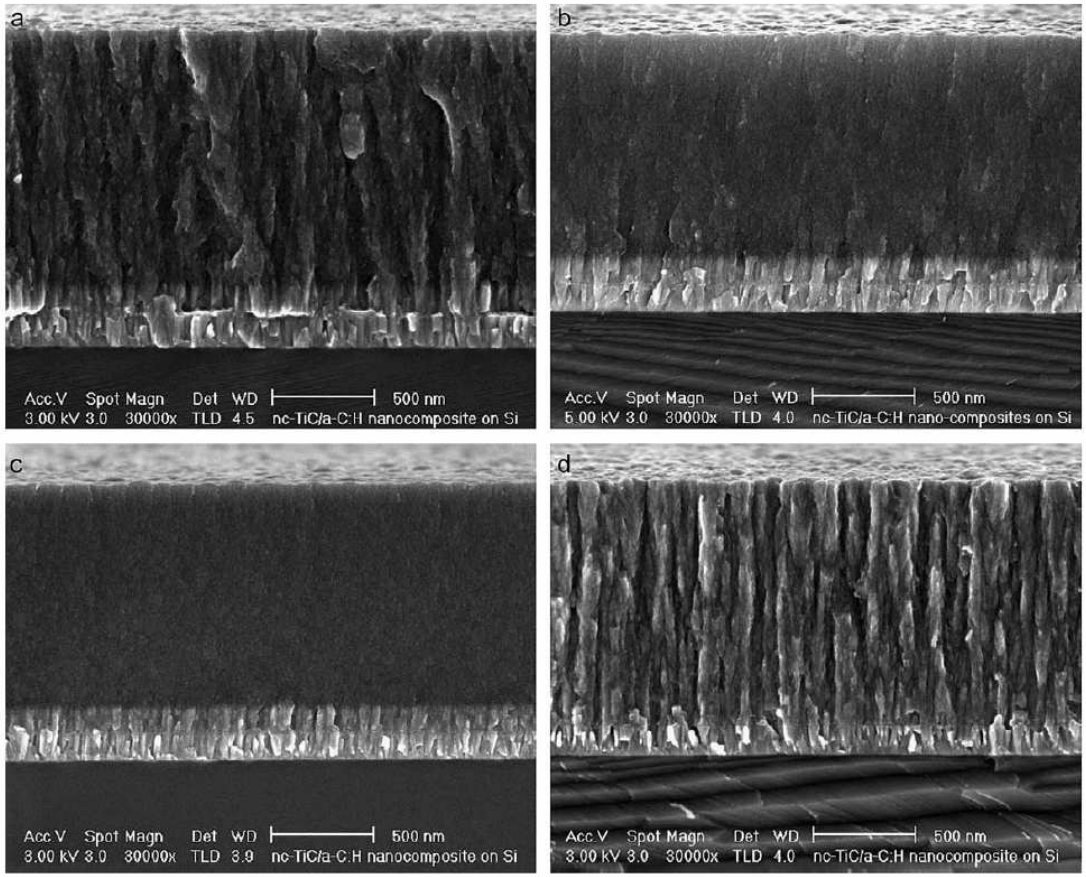

Fig. 3. SEM micrographs of fractured cross-sections showing the transition from columnar to glassy structures of nc-TiC/a-C:H coatings deposited under different conditions: (a) 110 sccm C_2H_2 and −60 V bias; (b) 110 sccm C_2H_2 and −100 V bias; (c) 110 sccm C_2H_2 and −150 V bias and (d) 80 sccm C_2H_2 and −100 V bias.

Pei et al. (2005)

Revestimento nc-TiC/a-C

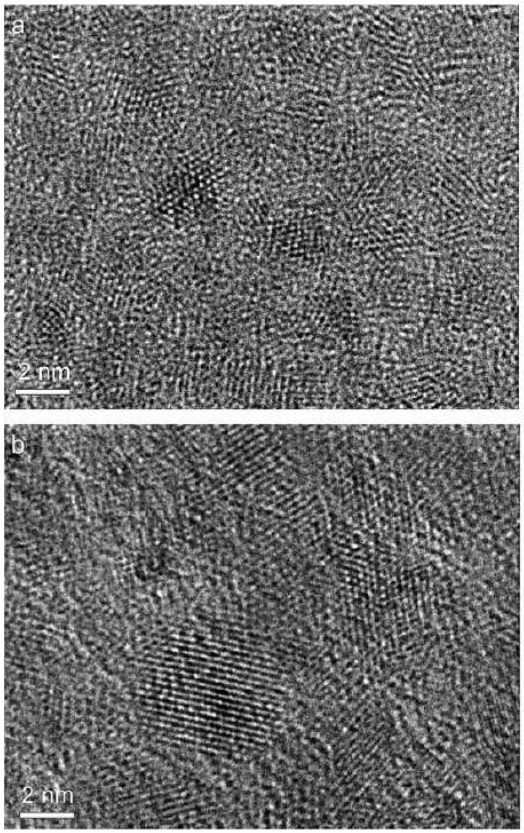

Fig. 4. HRTEM micrographs showing TiC nanocrystallites embedded in a-C:H matrix in nc-TiC/a-C:H nanocomposite: (a) coating HB3 with 17.84 at.% Ti and (b) coating HB5 with 31.75 at.% Ti.

Pei et al. (2005)

Nanoestruturação de superfícies

Nano region width = 22 μm;
Micron region width = 40 μm

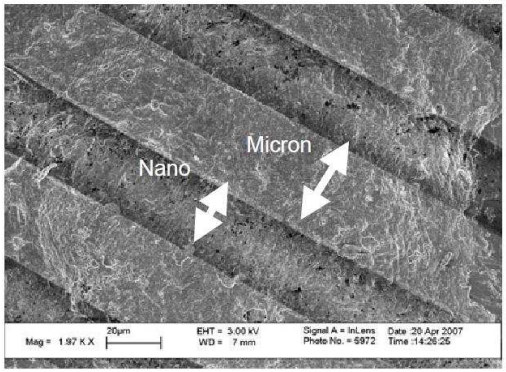

(g) Patterned Ti substrates
(scale bar = 20 μm)

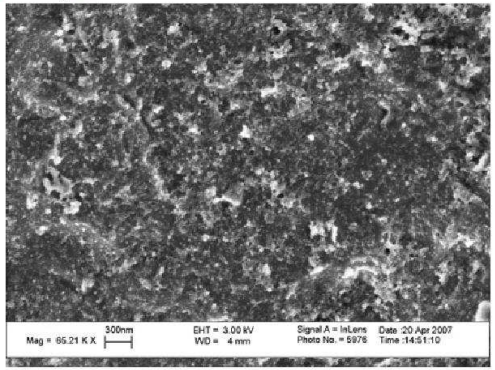

(h) Micron region on patterned Ti substrate
(scale bar = 300 nm)

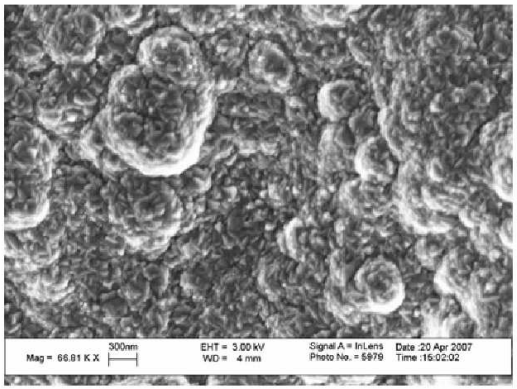

(i) Nano region on patterned Ti substrate
(scale bar = 300 nm)

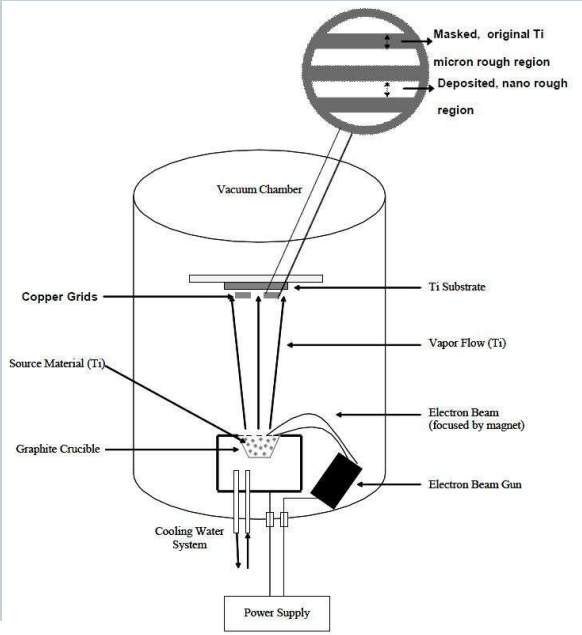

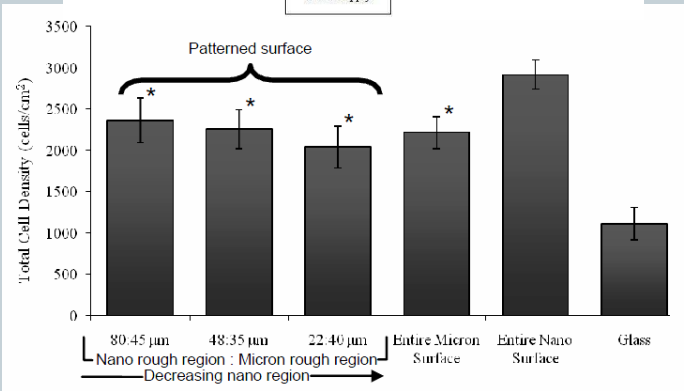

Pucket et al. 2008

Sensitividade a modificações superficiais de biomateriais

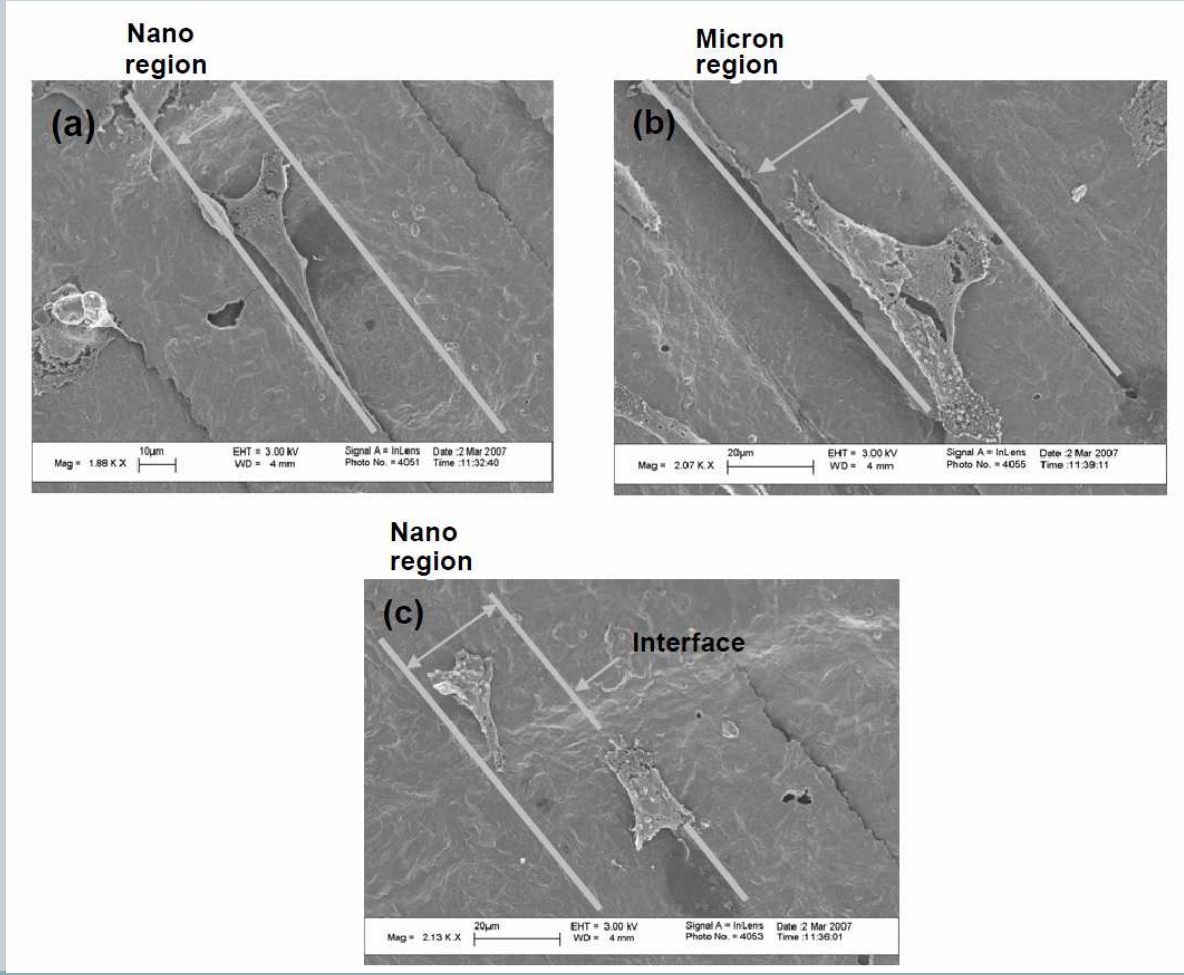

Pucket et al. 2008

Sensitividade a modificações superficiais de biomateriais

- Nanolitografia por Feixe de Elétrons para modificação superficial visando aumento da biocompatibilidade.
- Limite de sensibilidade por fibroblastos ~ 35 nm

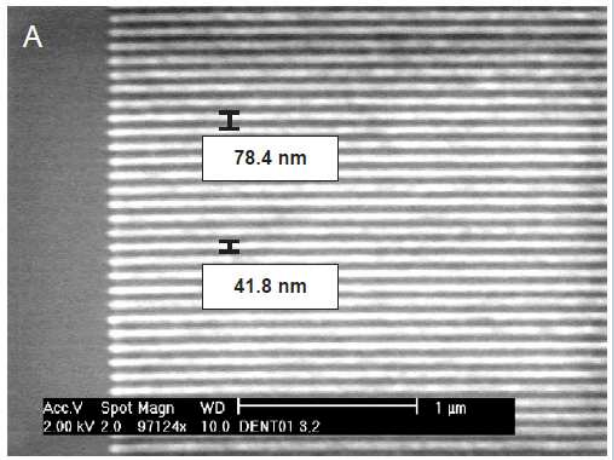

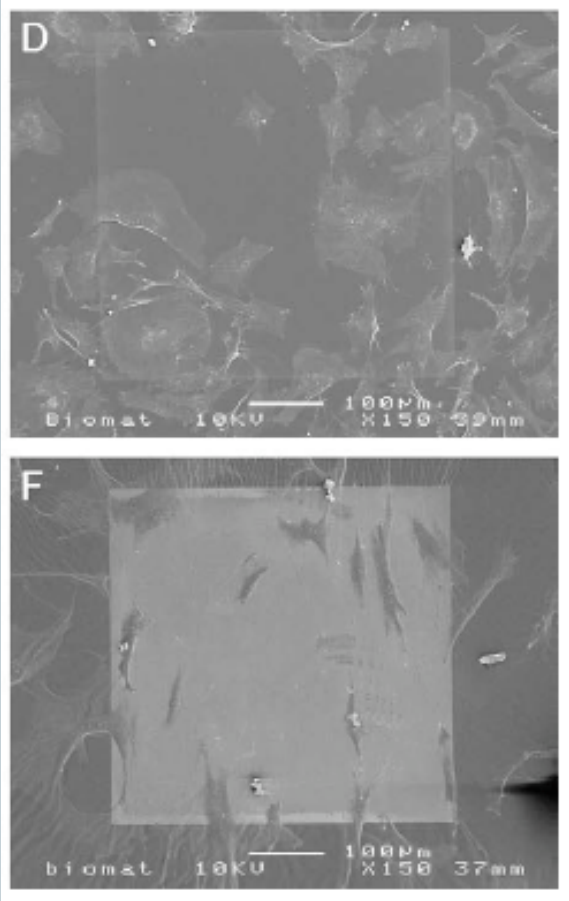

Máscaras feitas por litografia de feixe de elétrons para identificar o limite de sensibilidade dos fibroblastos.
D – 15 nm
F – 35 nm

Loesberg et al. Biomaterials V. 28 (2007) p. 3944-3951

Nanocordas

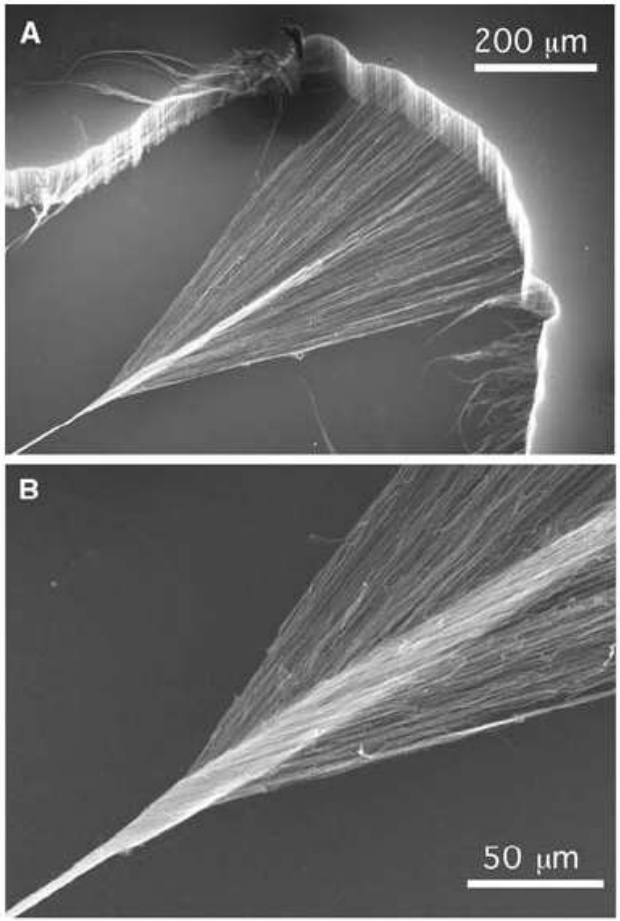

Fig. 1. (A and B) SEM images, at two different magnifications, of a carbon nanotube yarn in the process of being simultaneously drawn and twisted during spinning from a nanotube forest outside the SEM. The draw twist process was interrupted and the sample was transferred to a SEM for image recording. A forest strip (width ~600 μm) formed the pictured twisted yarn, 3.2 μm in diameter (fig. S2). The MWNTs, ~10 nm in diameter with length 10,000 times their width, form small bundles of a few nanotubes each in the forest, with individual nanotubes moving in and out of different bundles. The three-dimensional connectivity caused by intermittently switched bundling, visible in SEM micrographs, is believed to be important for the spinning process.

Zhang, M. et al.
Science 306, 2004, p. 1358-1361

Nanocordas

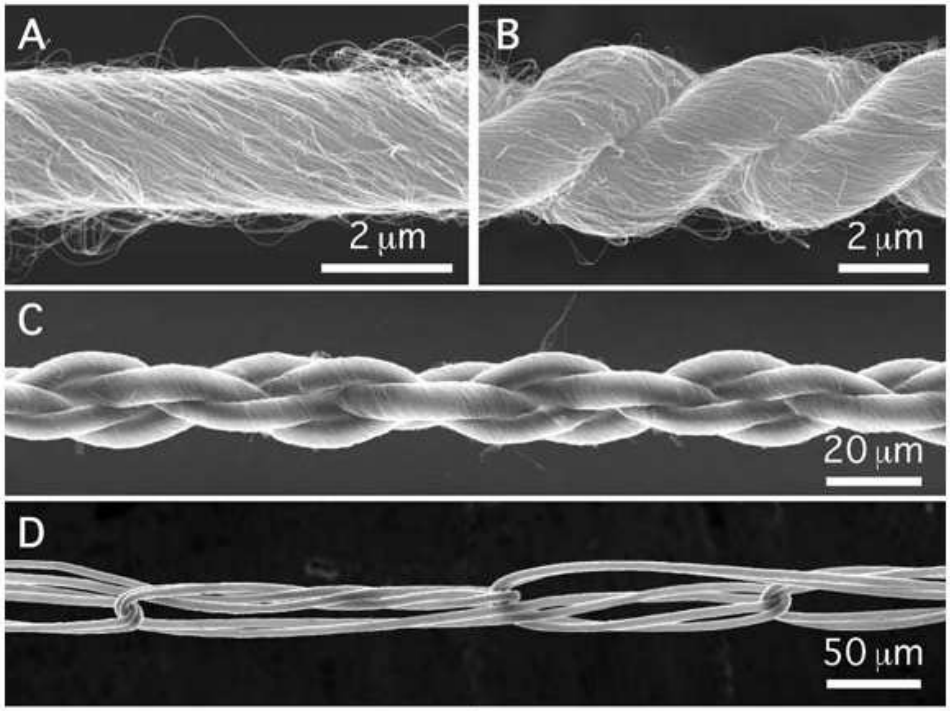

Fig. 2. SEM images of (A) singles, (B) two-ply, and (C) four-ply MWNT yarns, as well as (D) knitted and (E) knotted MWNT yarns.

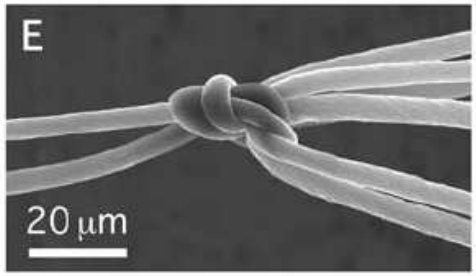

Zhang, M. et al.
Science 306, 2004, p. 1358-1361

Nanocordas

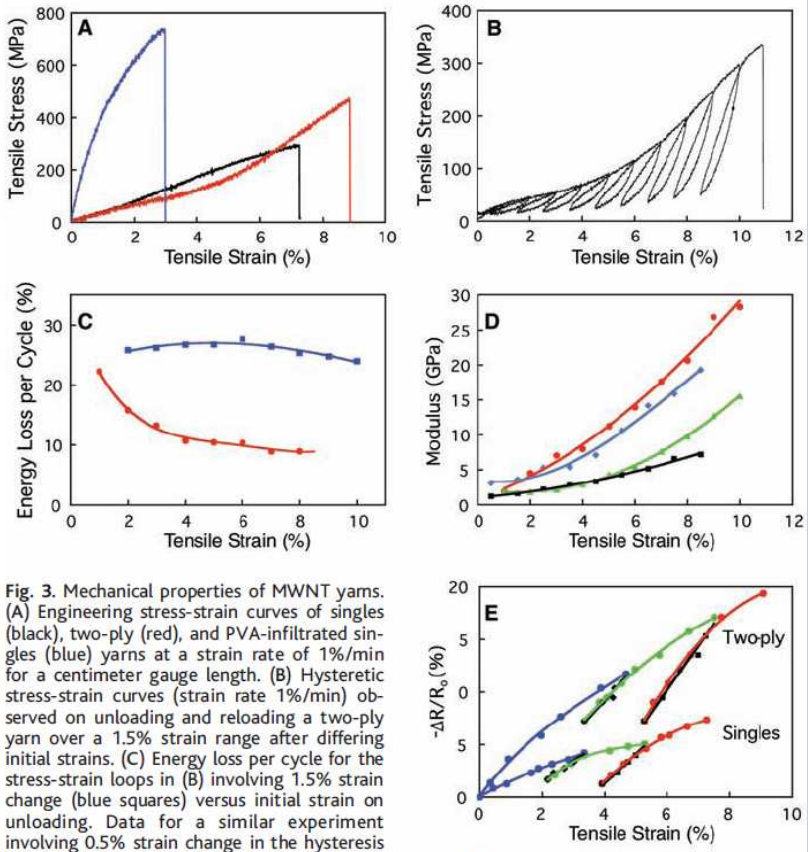

Fig. 3. Mechanical properties of MWNT yarns. (A) Engineering stress-strain curves of singles (black), two-ply (red), and PVA-infiltrated singles (blue) yarns at a strain rate of 1%/min for a centimeter gauge length. (B) Hysteretic stress-strain curves (strain rate 1%/min) observed on unloading and reloading a two-ply yarn over a 1.5% strain range after differing initial strains. (C) Energy loss per cycle for the stress-strain loops in (B) involving 1.5% strain change (blue squares) versus initial strain on unloading. Data for a similar experiment involving 0.5% strain change in the hysteresis loops are also shown (red circles). (D) Effective yarn moduli calculated for the stress-strain loops shown in (B) versus total tensile strain. Red circles and black squares are the effective moduli for the beginning and end of unloading, respectively; blue diamonds and green triangles are those for the beginning and end of reloading, respectively. (E) Percent change in diameter and length of a two-ply yarn (top) and a singles yarn (bottom) measured during yarn stretching in a SEM. Symbols: blue circles, initial stretch; black diamonds, first stress decrease; green circles, second stress increase; black squares, second stress decrease; red circles, stress increase until yarn rupture. Curves in (C) to (E) are guides for the eye.

Zhang, M. et al.
Science 306, 2004, p. 1358-1361

Nanofios de Si Células Fotovoltaicas

- Objetivos: flexibilidade mecânica, aumento na absorção e diminuição na quantidade de material

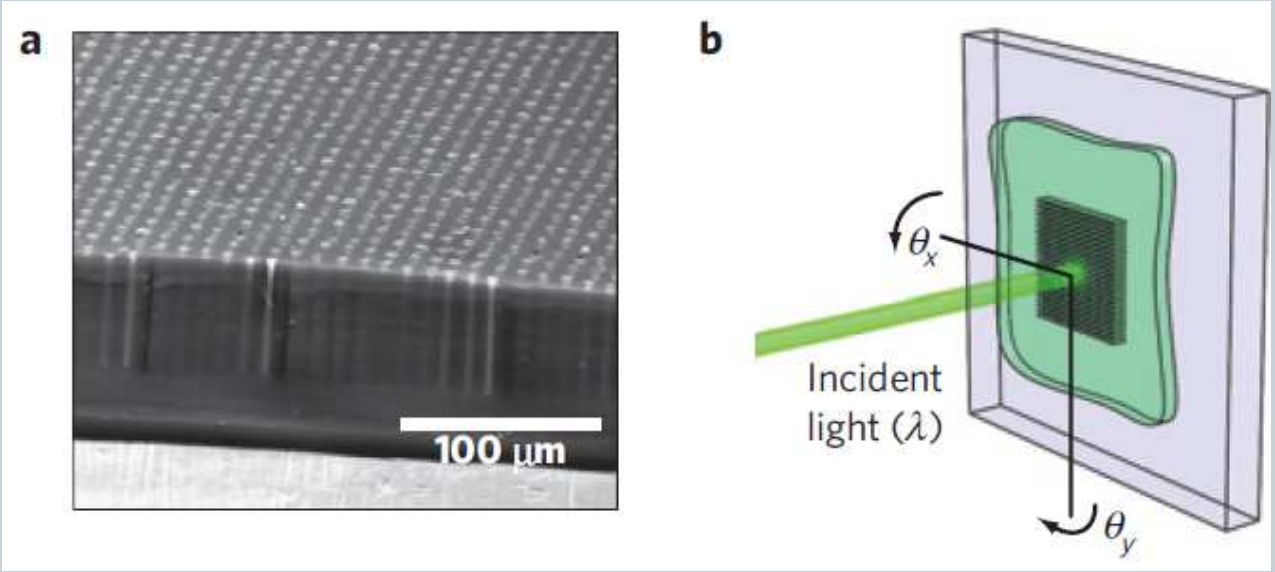

Nanofios de Si Células Fotovoltaicas

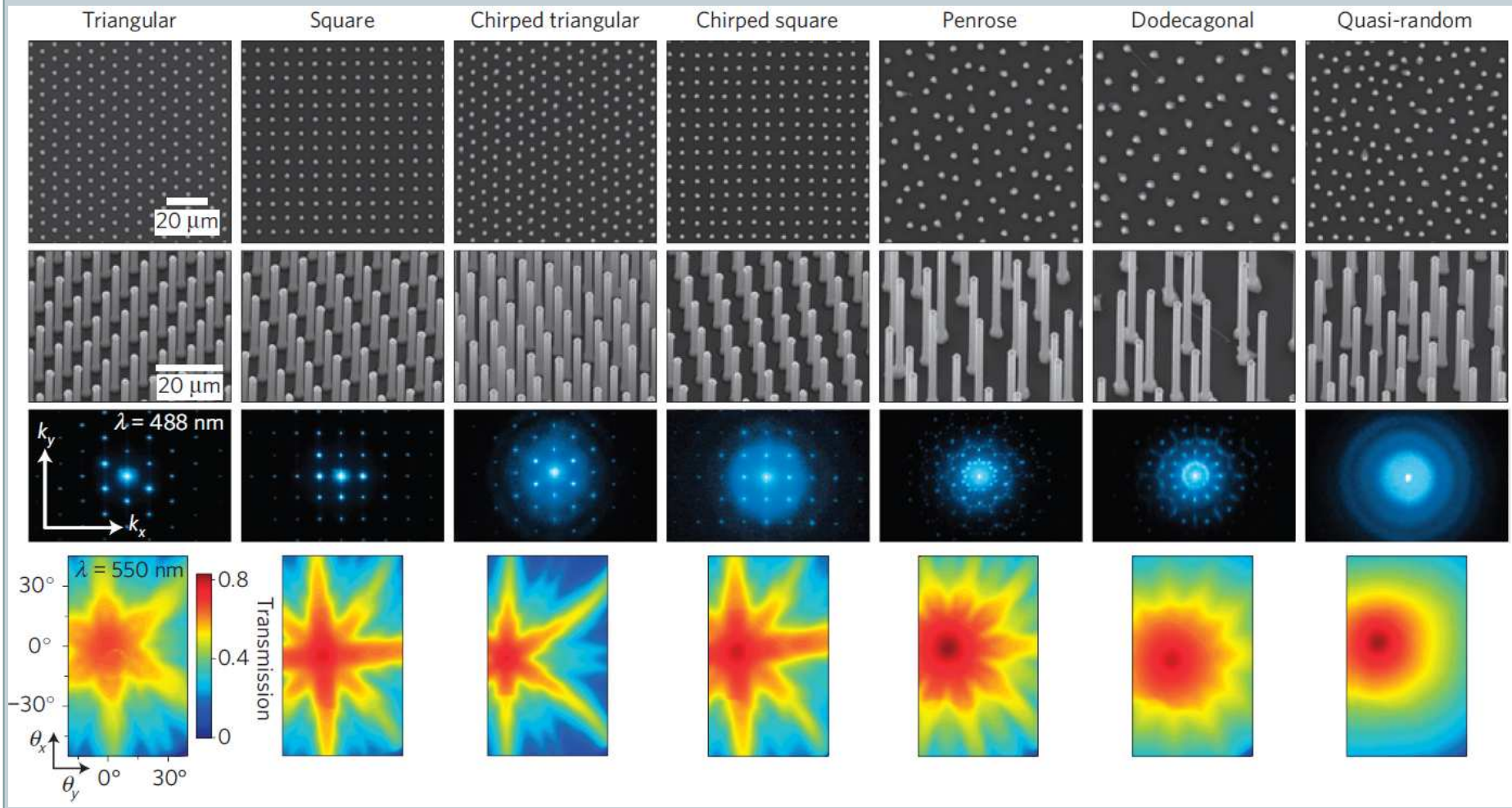

Cristais Fotônicos

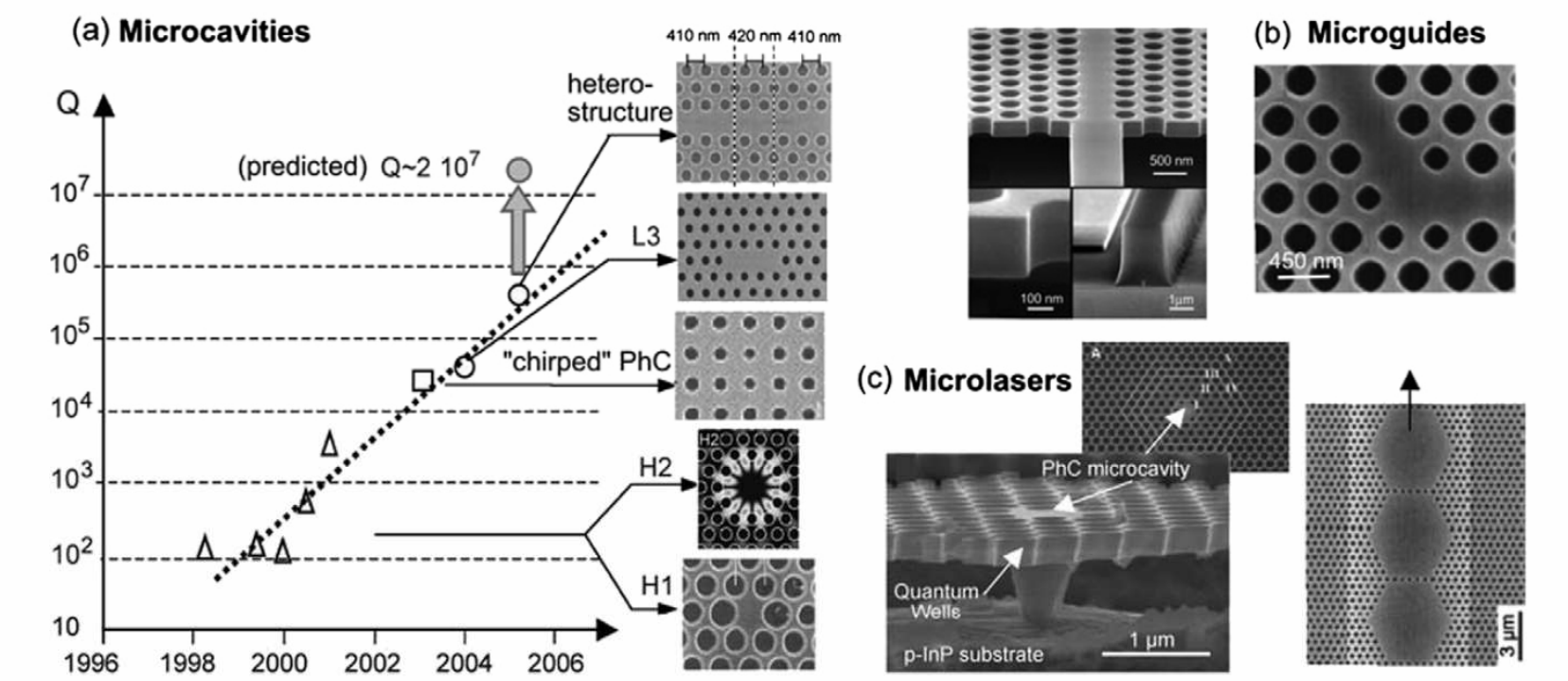

Fig. 1. Photonic crystal micro-devices. (a) Evolution of the Q-factor of photonic crystal microcavities during the last decade. (b) Left: W1 waveguide fabricated in the silicon membrane technology and formed by one row of missing holes in a hexagonal lattice of holes [33]. (b) Right: Light bent, realized in the same technology [5]. (c) Left: First electrically driven photonic crystal microcavity laser fabricated in the InP technology, the light being emitted vertically [6]. (c) Right: Edge-emitting coupled-cavity-waveguide laser fabricated on InP substrate [42].

Lourtioz 2008

Cristais Fotônicos

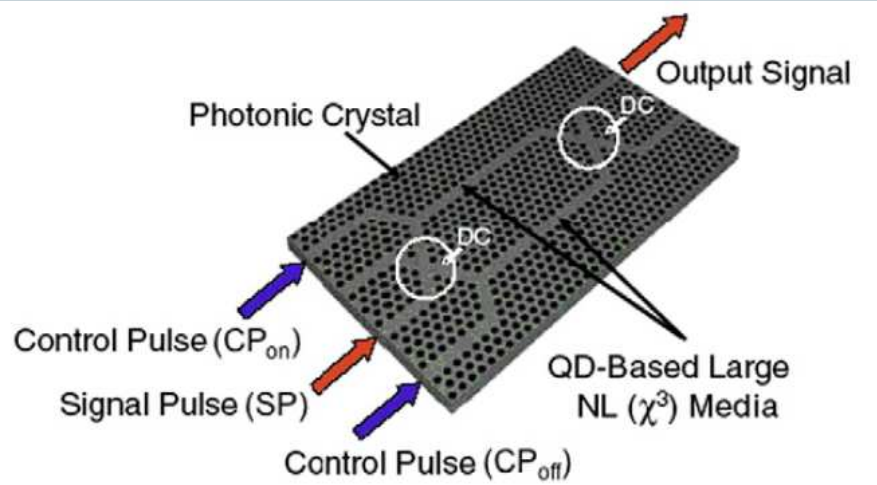

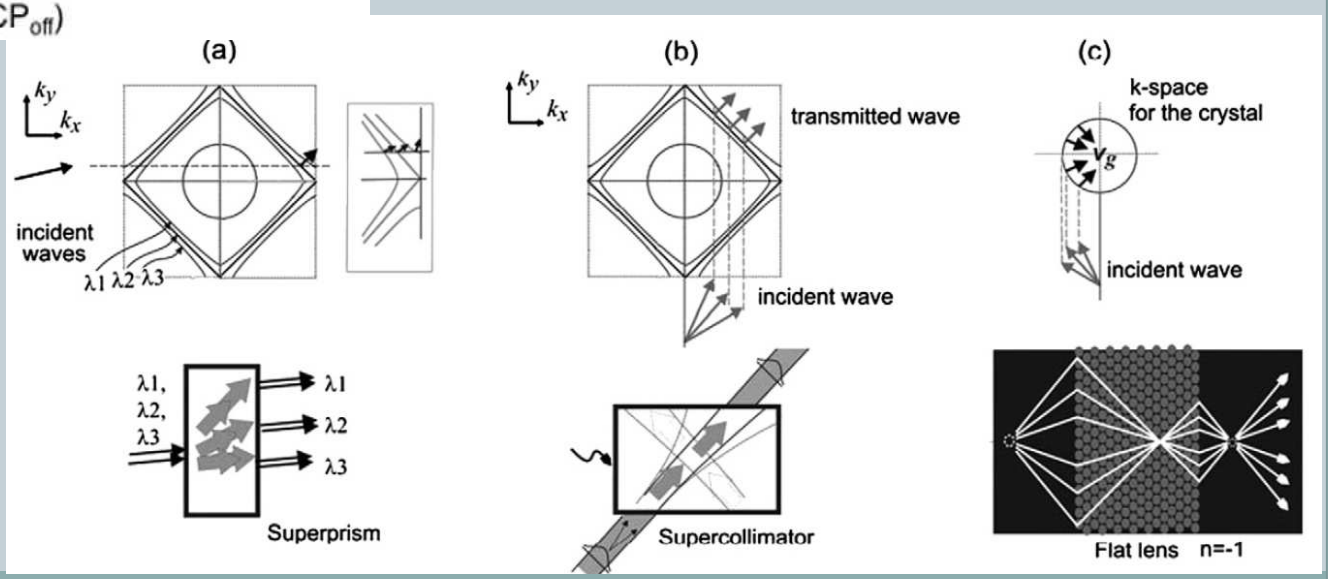

Cristais Fotônicos

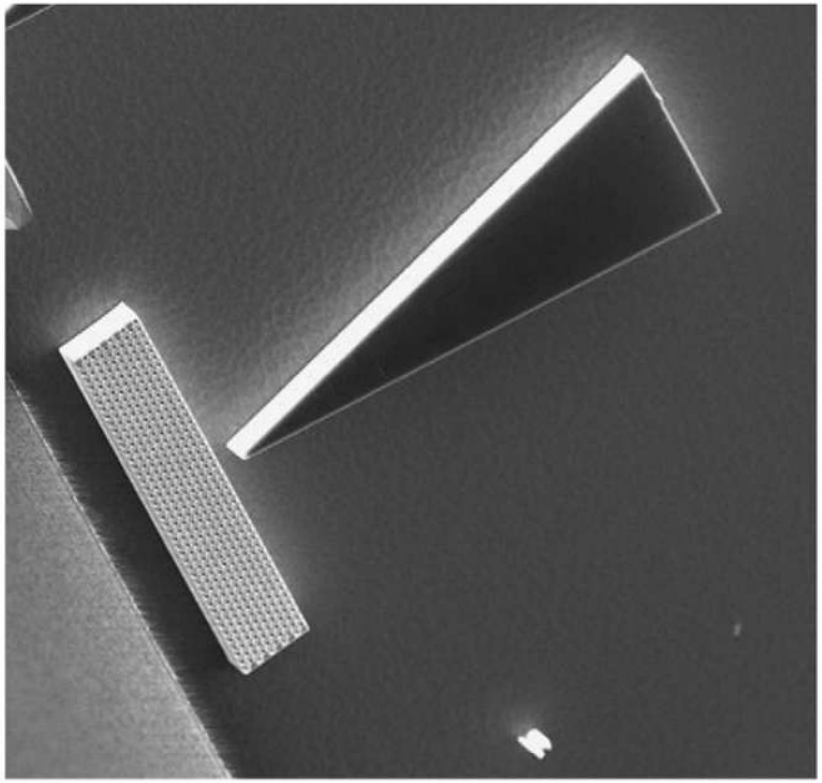

Fig. 16. SEM of a flat lens fed by a tapered optical waveguide.

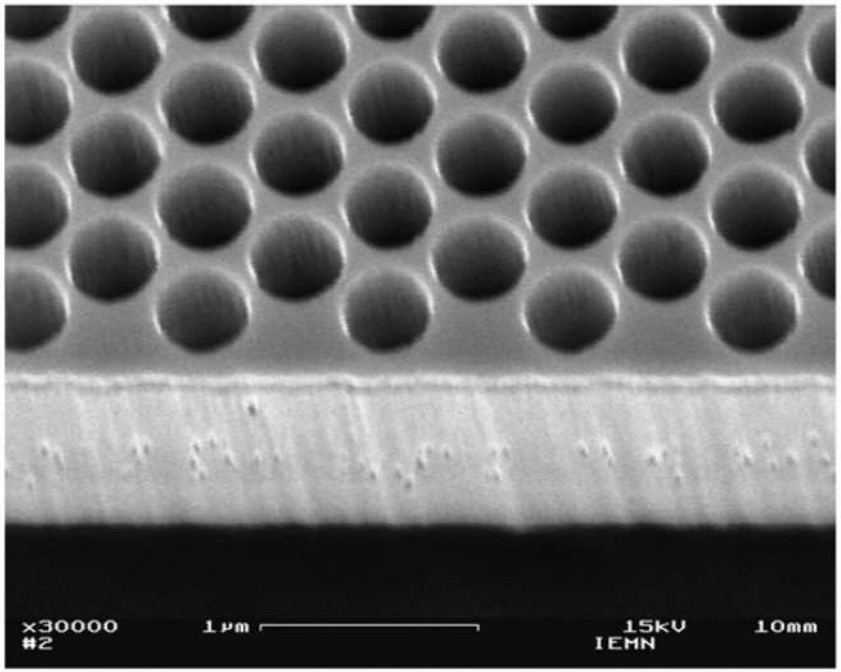

Fig. 15. Close up view of a hole array.

Lippens 2008

Metamateriais

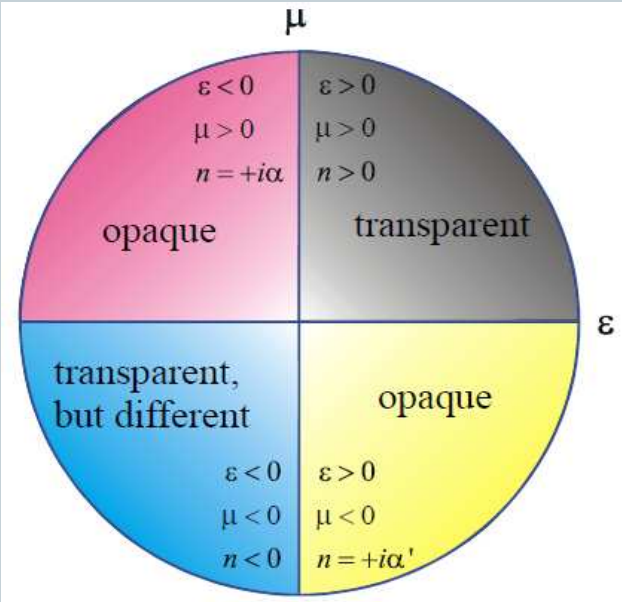

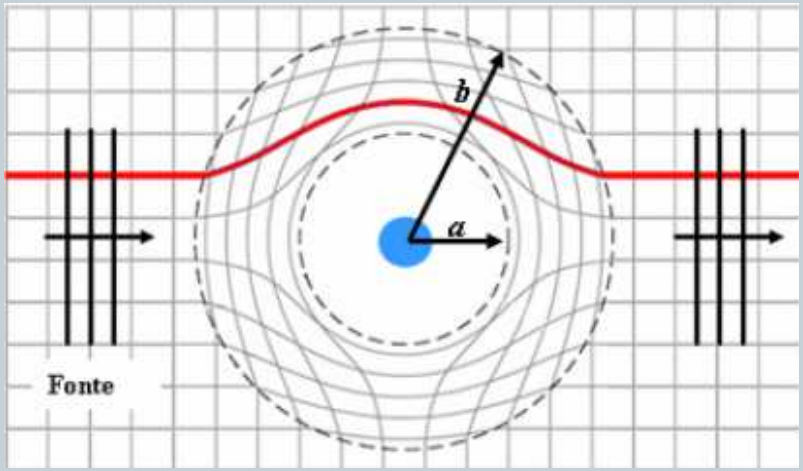

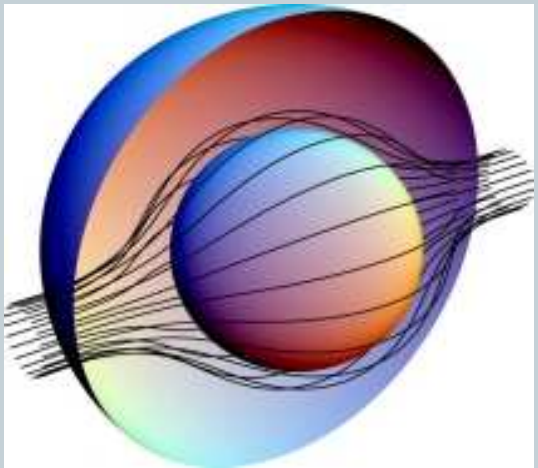

Uma aplicação: invisibilidade eletromagnética

Macedo 2008

Metamateriais

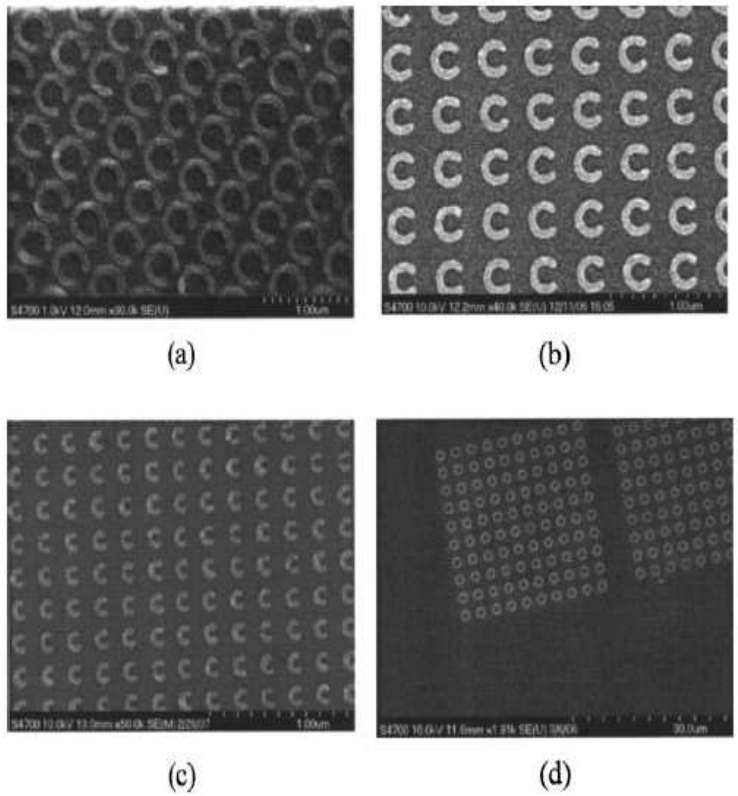

FIG. 2. Scanning electron micrographs of split ring arrays with radii (a) 215 nm, (b) 130 nm, and (c) 60 nm. (d) Scanning electron micrograph of complete 125 nm radius rings.

Sheridan et al. 2007

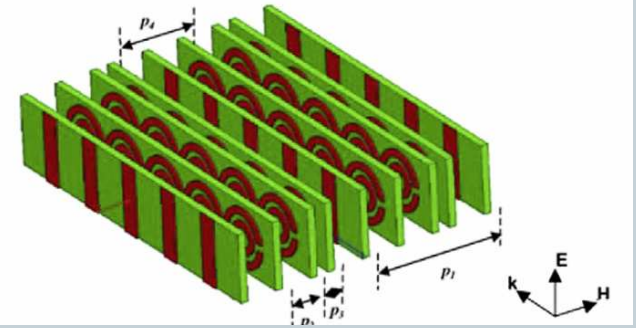

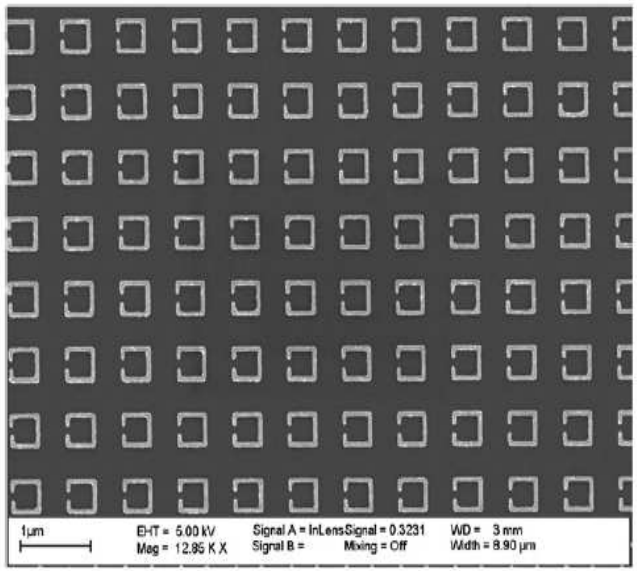

Fig. 11. SEM of a plasmon resonator array.

Lippens 2008

Metamateriais 3D

Michael , S. R. et al. Nature Materials 7 (2008) p. 543-546

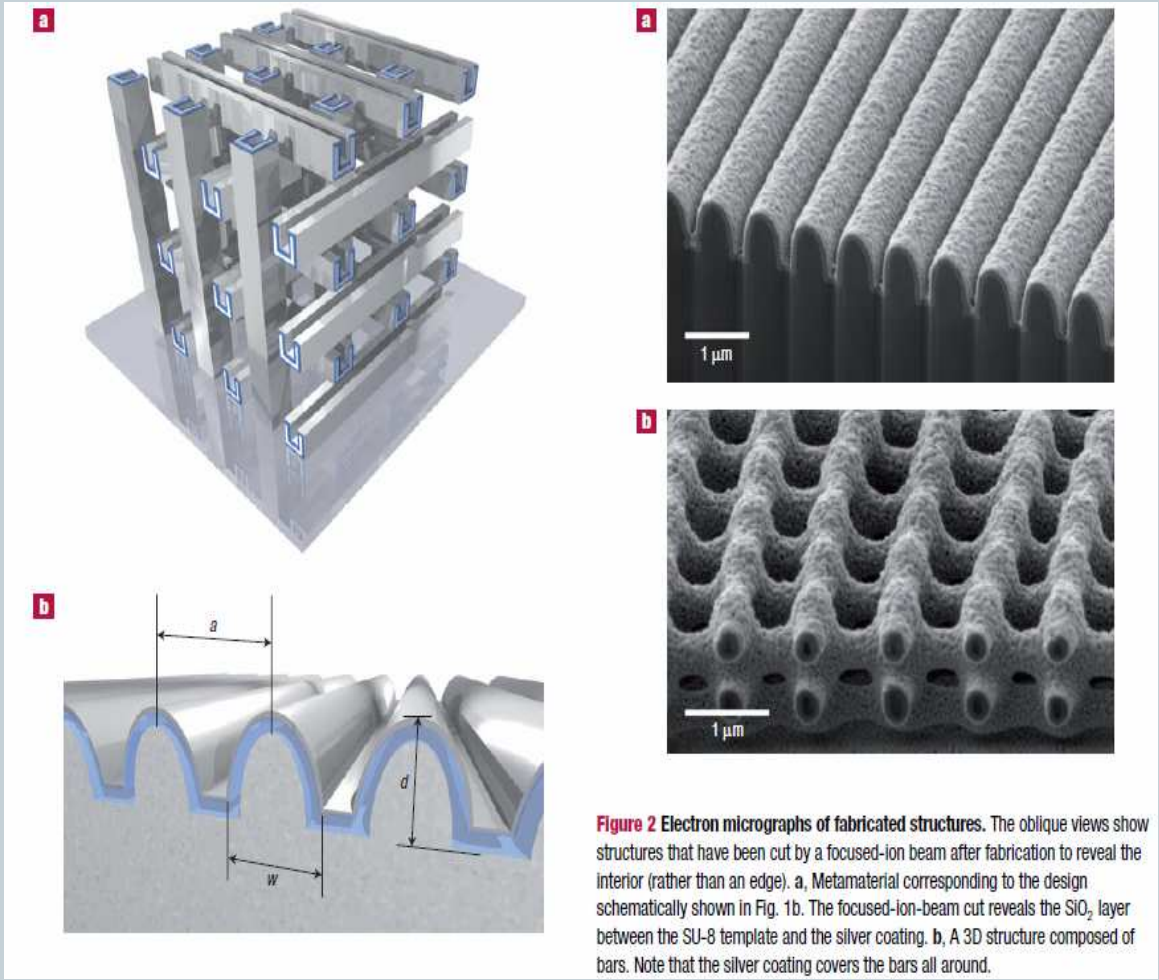

Figure 2 Electron micrographs of fabricated structures. The oblique views show structures that have been cut by a focused-ion beam after fabrication to reveal the interior (rather than an edge). **a**, Metamaterial corresponding to the design schematically shown in Fig. 1b. The focused-ion-beam cut reveals the SiO_2 layer between the SU-8 template and the silver coating. **b**, A 3D structure composed of bars. Note that the silver coating covers the bars all around.

Estruturas Quase-periódicas

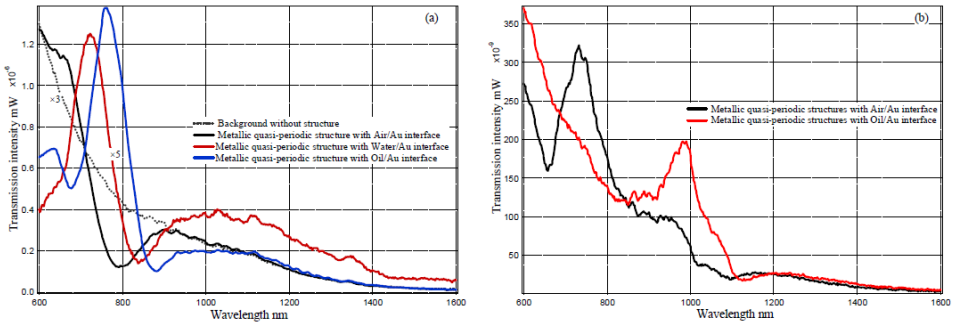

Fig. 3. The transmission spectra of the fabricated metallic quasi-periodic structures. (a) the quasi-periodic structures with three exposures at a rotation angle of 40° (the angle θ is 35°);(b)the quasi-periodic structures with four exposures at a rotation angle of 30° (the angle θ is 22°).

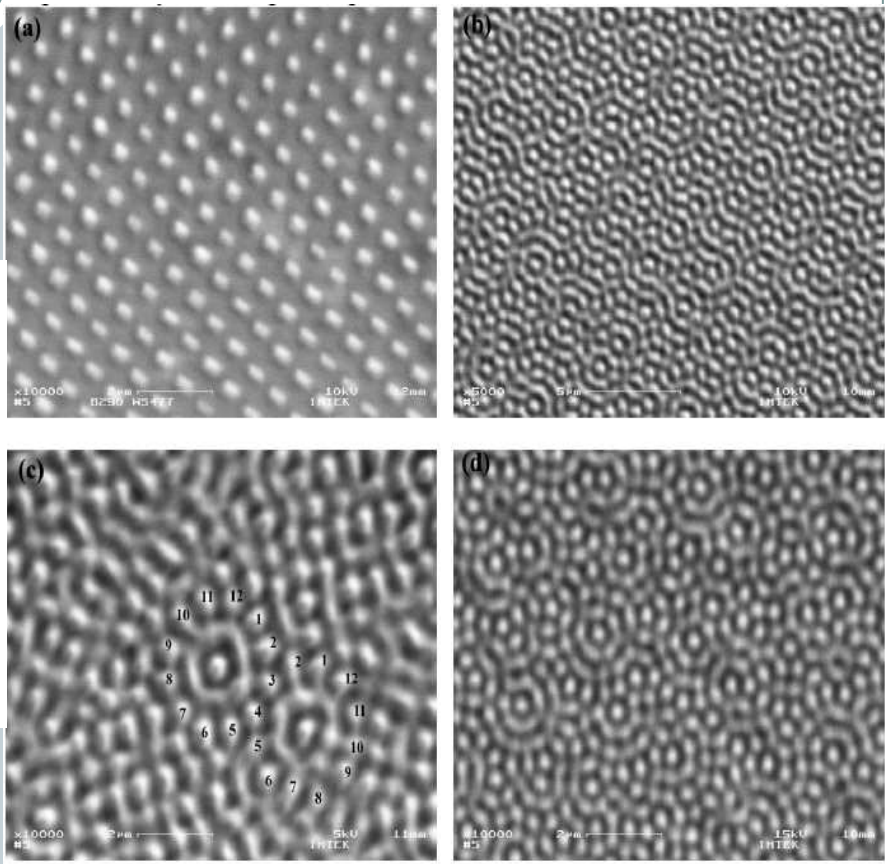

Fig. 2. SEM micrographs of fabricated metallic structures using the exposure wavelength at 442nm, (a),(b)&(c) the angle θ is 22°. (a) the fundamental 2D structures; (b) the quasi-periodic structures with three exposures at a rotation angle of 40°; (c) the quasi-periodic structures with four exposures at a rotation angle of 30°; (d) the quasi-periodic structures with three exposures at a rotation angle of 40° (the angle θ is 35°).

Wang 2008

Metamateriais Nanoporosos

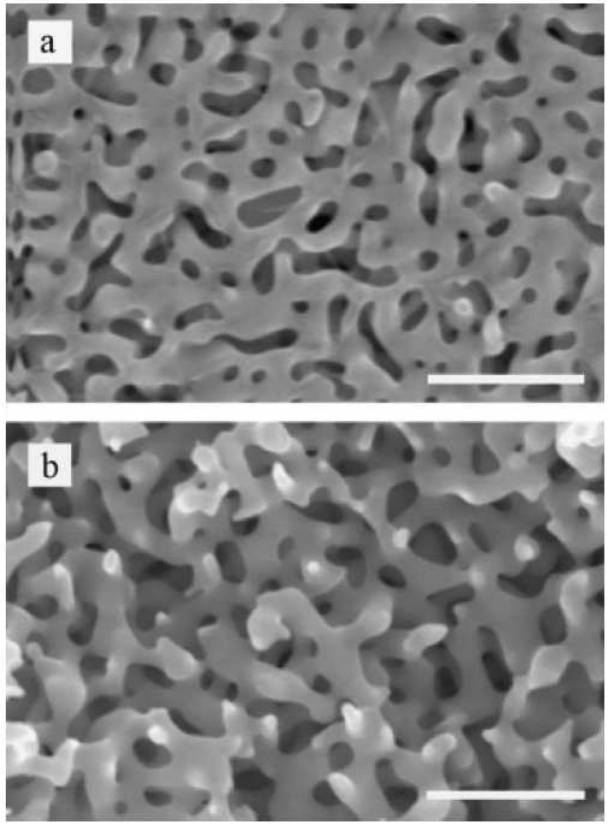

Figure 1. a) Plane-view, and b) cross-sectional scanning electron microscopy (SEM) images showing the characteristic spongelike open-cell foam morphology of np-Au. The material is very homogeneous and exhibits nanometer-sized pores and ligaments, the latter with a length-to-diameter aspect ratio close to one. The scale bars are 300 nm.

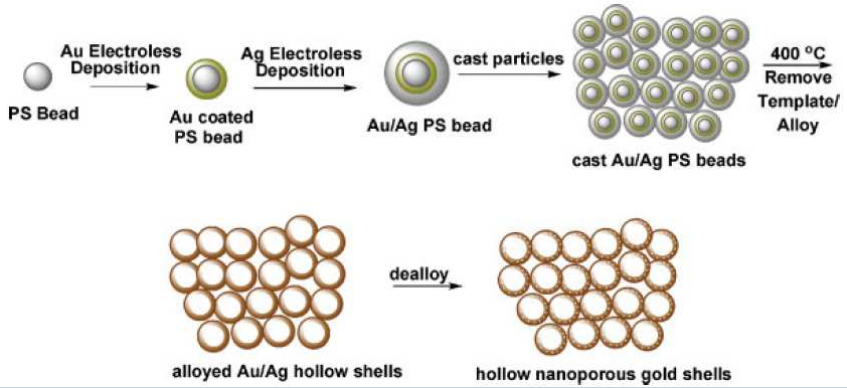

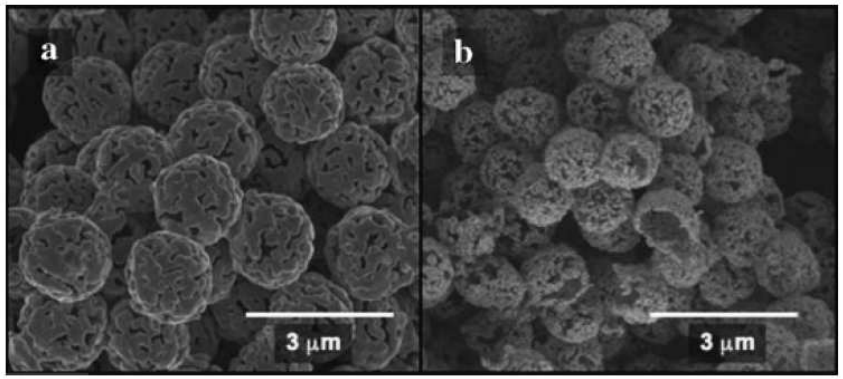

Figure 6. a) Fracture surface of a monolith containing hollow 1 μm $Ag_{0.7}Au_{0.3}$ shells before dealloying (density 1 g cm^{-3}). b) Fracture surface of a monolith containing hollow 1 μm nanoporous Au shells after dealloying (density 0.45 g cm^{-3} or 2.3% of the full density of Au).

Biener et al. 2008

EBSD

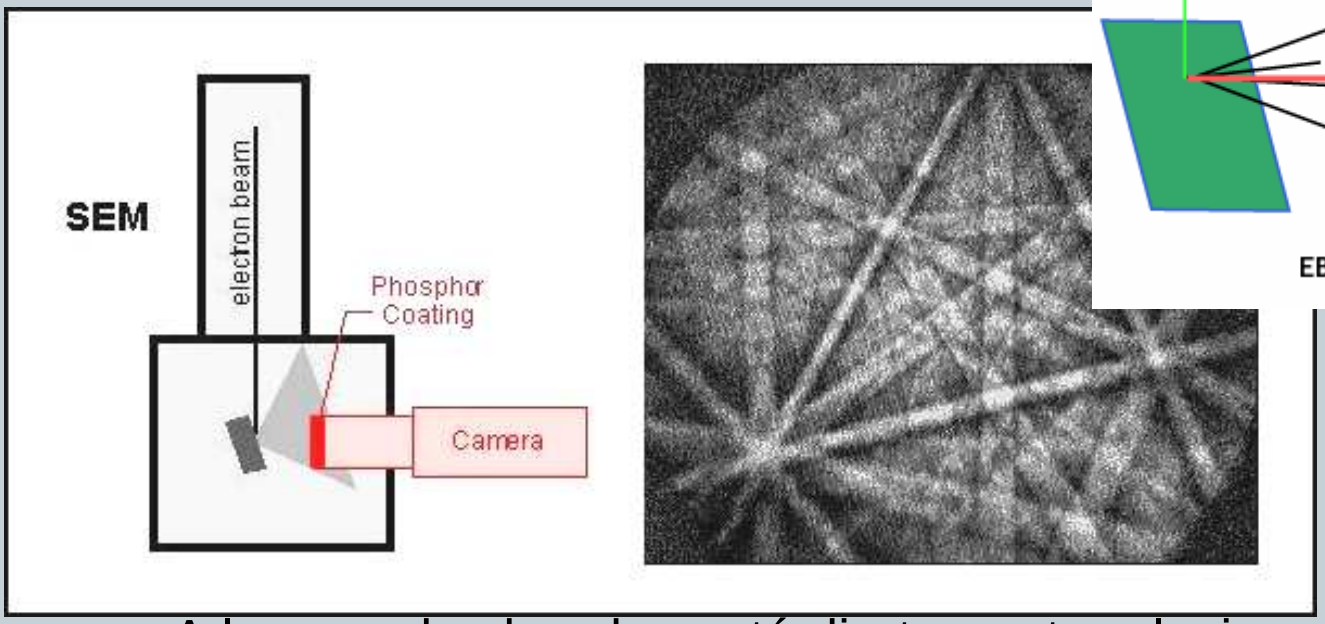

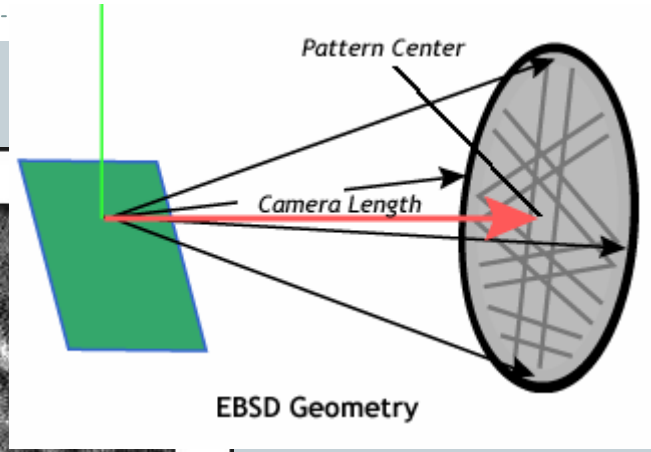

- A largura das bandas está diretamente relacionada ao espaçamento interplanar.
- O ângulo entre as bandas corresponde ao ângulo entre os planos cristalinos.
- A posição das bandas está ligada à posição dos planos.

NiCo Nanoestruturado Eletrodepositado

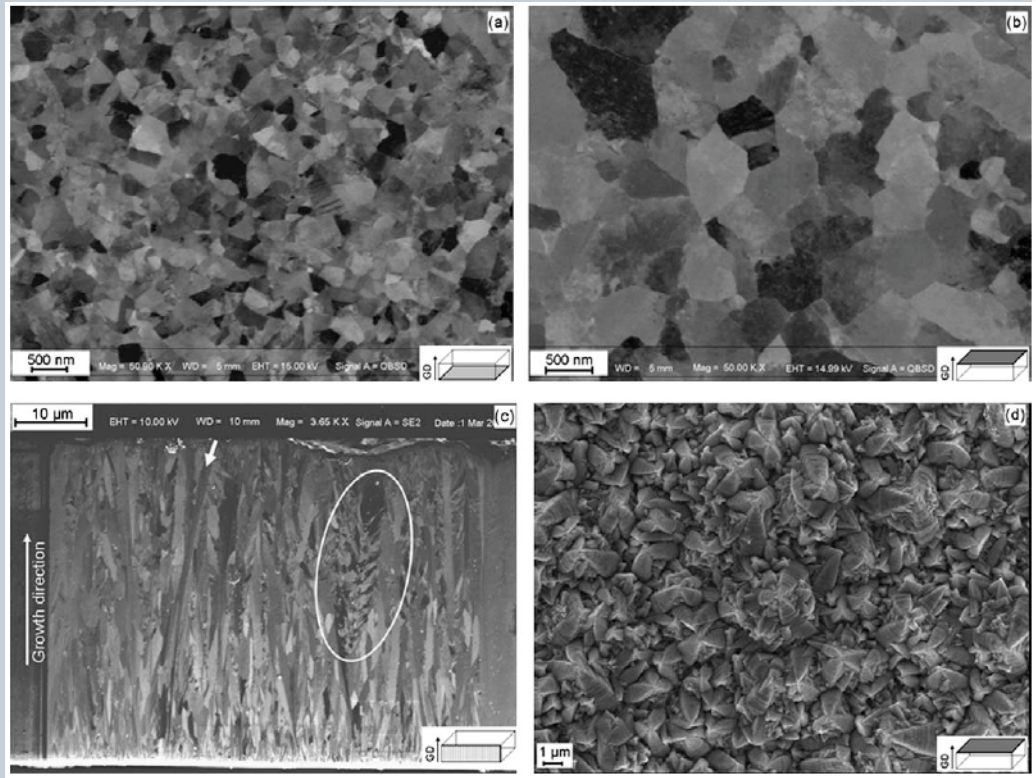

Bastos et all 2006

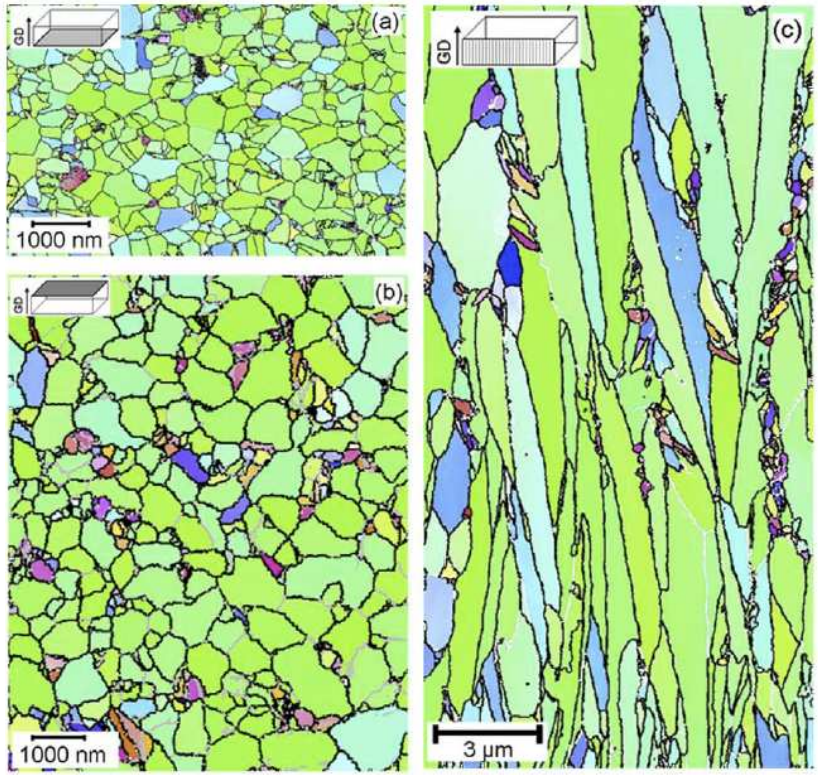

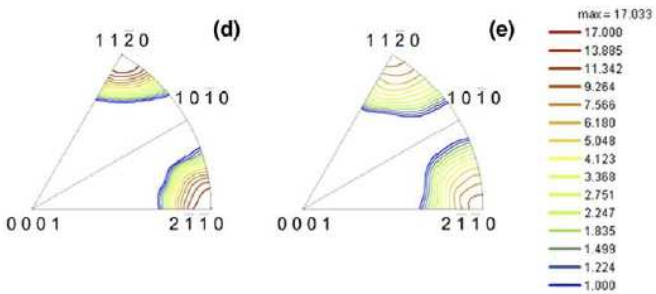

NiCo Nanoestruturado Eletrodepositado

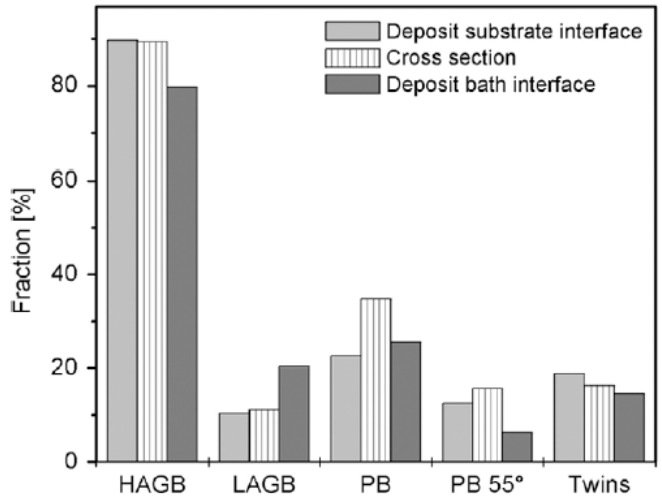

Bastos et all 2006

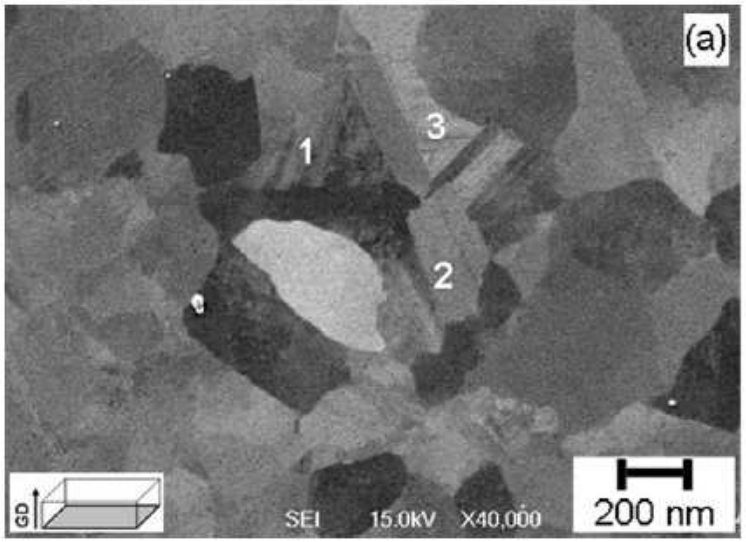

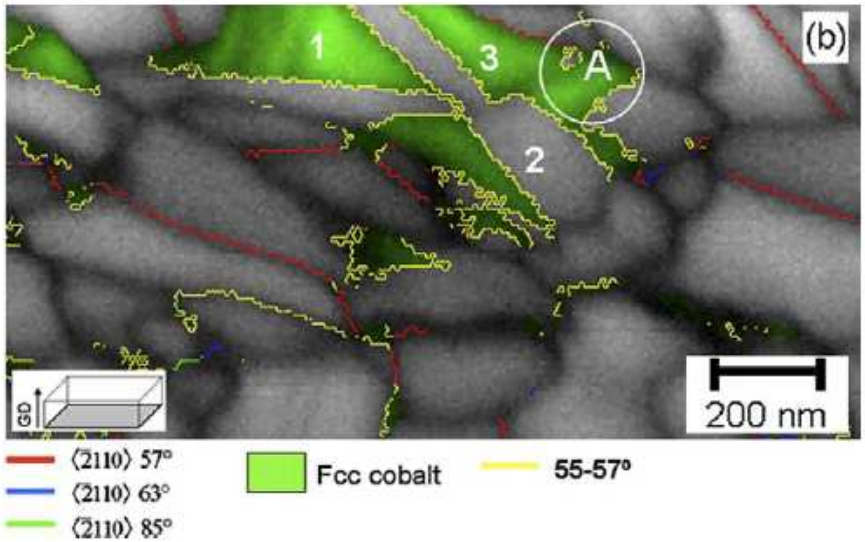

Referências

- Goldstein, J. I. et alli., “Scanning Electron Microscopy and X-Ray Analysis”, Ed. Plenum, New York, 2003.
- Goodhew, P. J. et all, “Electron Microscopy and Analysis”, Ed. Taylor & Francis, London, 2001.
- Lippens, D. “Metamaterials and infra-red applications” C. R. Physique 9 (2008) p. 184-196.
- Wang, Y. “Fabrication and characterization of metallic quase-periodic structures”, Optics Express V16, N2 (2008) p. 1090-1095.
- Lourtioz, J. M. C. R. “New concepts for nanophotonics and nano-electronics – Photonic crystals and metamaterials”, Physique 9 (2008) p. 4-15
- Biener, J. et al. “Nanoporous plasmonic metamaterials”, Advanced Materials 20 (2008) p. 1211-1217.
- Sheridan, A. K. et al. *Fabrication and tuning of nanoscales metallic ring and split-ring arrays*. Journal of Vacuum Science and Technology B 25/6 (2007) p. 2628-263.
- Michael , S. R. et al. *Photonic metamaterials by direct laser writing and silver chemical vapour deposition*. Nature Materials 7 (2008) p. 543-546.
- Thune, E. *Nanostructured sapphire vicinal surfaces as templates for the growth of self-organized oxide nanostructures*. Applied Surface Science 256 (2009) p. 924-928.
- Loesberg et al. Biomaterials V. 28 (2007) p. 3944-3951
- Zhang, M. et al. Science 306, 2004, p. 1358-1361

Referências

- Bastos, A. et al.. Acta Materialia 54 (2006) p. 2451-2462.
- Kelzenberg, M. D. et al.. Nature Materials 9 (2010) p. 239-244
- J. Macêdo. *Formalismo FDTD para a modelagem de meios dispersivos apresentando anisotropia biaxial*. Dissertação. Universidade de São Paulo, 90 p, 2008.
- Pei, Y. T. et al. *Nanostructured TiC/a-C coatings for low friction and wear resistant applications.* Surface & Coatings Technology 198 (2005) p. 44-50.
- Puckett, s. et al. International Journal of Nanomedicine 3 (2008) p. 229-241.

André L. Pinto

pinto@cbpf.br

- Obrigado pela atenção

INTERNATIONAL
MICROSCOPY CONGRESS
IMC17
September 19-24
2010 - RIO - BRAZIL